Elisabeth Dovalil, BSc

Optical Investigations of the Internal Structure of the Glass System Na$_2$O-B$_2$O$_3$-Al$_2$O$_3$ (NABAL)

MASTER'S THESIS

to achieve the university degree of

Diplom-Ingenieurin

Master's degree programme: Technical Chemistry

submitted to

Graz University of Technology

Supervisor

Ao.Univ.-Prof. Dipl.-Ing. Dr.techn. Karl Gatterer

Institute of Physical and Theoretical Chemistry

Graz, October 2019

AFFIDAVIT

I declare that I have authored this thesis independently, that I have not used other than the declared sources/resources, and that I have explicitly indicated all material which has been quoted either literally or by content from the sources used. The text document uploaded to TUGRAZ online and UNIGRAZ online is identical to the present master's thesis.

_____
Date

_____
Signature

EIDESSTATTLICHE ERKLÄRUNG

Ich erkläre an Eides statt, dass ich die vorliegende Arbeit selbstständig verfasst, andere als die angegebenen Quellen/Hilfsmittel nicht benutzt, und die den benutzten Quellen wörtlich und inhaltlich entnommenen Stellen als solche kenntlich gemacht habe. Das in TUGRAZ online beziehungsweise UNIGRAZ online hochgeladene Textdokument ist mit der vorliegenden Diplomarbeit ident.

_____
Datum

_____
Unterschrift

Acknowledgement

Abstract

Rare-earth doped glasses have a broad range of applications, especially in optoelectronic devices like solid-state lasers. The modification of the energy levels of the rare-earth ion in the host material is not only interesting for those applications, but also for the elucidation of the internal glass structure as a complementary analysis tool to other experimental techniques like (MAS-)NMR or IR spectroscopy. In the present work the rare-earth ions Eu^{3+} and Nd^{3+} were used as structural probes in glasses of binary sodium borate and ternary sodium aluminium borate glasses. Changes in the optical spectra were interpreted in terms of internal structural changes that occur in the host glass materials in dependence of the composition of the oxide glass. Therefore, binary and ternary glasses of the Na_2O-B_2O_3-Al_2O_3 system (NABAL glasses) have been prepared and investigated by luminescence and absorption spectroscopy. Additionally, the densities, molar volumes and packing ratios were determined and the optical basicity and the substructure amounts were calculated. The results were compared and completed with already existing results and theories from Gresch and Müller-Warmuth and Doweidar *et al.* with the aim to get a more complete mapping of the internal structure of NABAL glasses. The glass transformation region of the glass family proposed by Gresch and Müller-Warmuth was modified. Further, the structural change at $Na_2O \sim 30$ mol% proposed by Gresch and Müller-Warmuth could be confirmed by the optical investigation. These results are also in accordance with the Krogh-Moe model for borate glasses. Also, the determined densities are correspond to the results of Doweidar *et al.*

Kurzfassung

Seltenerd-dotierte Gläser werden für viele verschiedene Anwendungen verwendet, vor allem jedoch für optoelektronische Einrichtungen, wie zum Beispiel für Laser. Die Modifikation der Energie-Niveaus des Seltenerd-Ions in Wirt-Materialien ist jedoch nicht nur interessant für die genannten Anwendungen, sondern ebenso für die Strukturaufklärung von Gläsern als ergänzende Analysenmethode zu (MAS-)NMR oder IR Spektroskopie.

In der vorliegenden Arbeit wurden die Seltenerd-Ionen Eu^{3+} und Nd^{3+} als Strukturproben in binären Natriumborat-Gläsern und ternären Natrium-Boroaluminat-Gläsern verwendet. Es wurden die Veränderungen in den optischen Spektren hinsichtlich der von der Zusammensetzung der Gläser abhängigen Glasstruktur interpretiert. Dafür wurden binäre und tertiäre Gläser des Na_2O-B_2O_3-Al_2O_3 Systems (NABAL Gläser) hergestellt und mittels Lumineszenz- und Absorptionsspektroskopie untersucht. Außerdem wurde die Dichte bestimmt, sowie das molare Volumen, die Packungsdichte, die theoretische optische Dichte und die Substrukturmengen berechnet. Die Ergebnisse wurden mit bereits existierender Literatur verglichen. Im Speziellen wurden dafür die Ergebnisse und Theorien von Gresch und Müller-Warmuth und Doweidar *et al.* herangezogen.

Die Glasbildungsregion von Gresch und Müller-Warmuth wurde modifiziert. Außerdem wurden die strukturellen Änderungen, die von Gresch und Müller-Warmuth bei 30 mol% Na_2O beschrieben wurden, ebenso beobachtet. Die Ergebnisse stimmen ebenso mit dem Krogh-Moe-Modell für Bor basierte Gläser überein. Bei den Dichtebestimmungen wurde das Dichteminimum von Doweidar *et al.* bestätigt.

Table of Contents

List of Abbreviations

(MAS-)NMR	(Magic-Angle-Spinning) Nuclear Magnetic Resonance
AS	Asymmetry ratio
BO	Bridging oxygen
CABAL	Calcium oxide borate oxide alumina oxide
e.g.	For example
ED	Electric-allowed dipole transition
FWHM	Full-with-at-half-maximum
h	Hour(s)
i.e.	That is to say
IR	Infrared
kcal	Kilocalorie(s)
MD	Magnetic-allowed dipole transition
min	Minute(s)
ms	Millisecond(s)
NABAL	Sodium oxide borate oxide alumina oxide
NBO	Non bridging oxygen
NIR	Near infrared
pm	Picometer(s)
RE	Rare earth
RT	Room temperature
s	Second(s)
UV	Ultraviolet
VIS	Visual
wt	Weight
XRD	X-Ray diffraction

List of Symbols

Λ_{th}	Theoretical optical basicity
$\chi_{XO_{\frac{x}{2}}}$	Proportion of oxygen ions each cation contributes
Δ	Crystal field strength
A	Area
a	Sum of the radii of cations and anions
F	Field strength
g	Gram(s)
J	Total angular momentum (orbital and spin) quantum number
L	Total orbital angular momentum quantum number
M	Molar mass
$N_3(B)$	Three-coordinated boron
$N_4(Al)$	Four-coordinated aluminium
$N_4(B)$	Four-coordinated boron
N_A	Avogadro constant
r_i	Radius of ion i
S	Total spin
T_f	Fictive temperature
T_g	Glass transition temperature
T_m	Melting point
V_m	Molar volume
x, y	Molfraction of oxides
Z_c	Valences of cation
α	Thermal coefficient
ρ	Density
$\Lambda\left(XO_{\frac{x}{2}}\right)$	Optical basicity of oxides of type X

I Introduction

Glasses are of considerable interest both in fundamental research as well as in technology. The history of this material is old and with the passage of time the number of applications expanded from decorative objects, architecture, transport, packaging, medical applications, antinuclear radiation containers and many others to the usage of the material for photosensitive devices used in solar cells, machine controls or optical fibres. [1],[2],[3]

Most of the commercially used glass materials are silicon glasses with SiO_2 as their main component. Other oxides used are B_2O_3 or P_2O_5. The structure of glass can be basically described as randomized three-dimensional network. To enter more in details, there is general agreement on the gross features of the relation between the glass composition and the structure in oxide glasses, but still the material has a lot of open questions concerning the organisation of the building blocks. The greatest contributions regarding the elucidation of the internal glass structure on borate glasses were made by Krogh-Moe around 1960 and 20 years later by Bray. Nowadays, there already exists a lot of literature on alkali borosilicate glasses, whereas the investigation of boroaluminate glasses is rather at an early stage. As it might be expected, the investigation of the glass structure gets even more complicated for multicomponent systems consisting of more than one oxide in comparison to single-component glasses. [4],[5],[6]

For the investigation of the structure of a network without a long-range order, one single technique is not enough to draw conclusions in terms of the organisation of the structure of the glass material. Therefore, information of various techniques must be combined to obtain a more complete mapping of the structure. For this purpose, experimental techniques like (Magic-Angle-Spinning- (MAS)) Nuclear Magnetic Resonance (NMR), Infrared (IR) or Raman spectroscopy are frequently applied. Additionally, UV-VIS spectroscopy can be performed. The latter requires the introduction of sensitive probes like rare earth (RE) ions into the samples. This technique is used in the present work to investigate the structure of ternary sodium boroaluminate (NABAL) glasses. The results are combined with already existing data of the literature derived from other experimental techniques, for example (e.g.) NMR. [6],[7]

The suitability of RE ions as structural probes arises from the unique electronic system of the RE elements as they have a partially filled 4f-shell, which is well shielded from external influences by the surrounding 5s- and 5p-shells. This basically leads to insensitivity towards the environment in which they are placed. Further, RE elements feature well defined sharp energy levels, the structure of which can be modified by the glassy environment. [8],[9]

For the present work, the trivalent RE ions of europium and neodymium are used. The usage of Eu^{3+} as structural probe in glasses has various advantages, like comparatively simple energy levels, which allow absorption and emission spectroscopy within the visible range.

Further, the correlations between the variations in the optical spectra of the trivalent europium ion and the structural changes in the host material are already well investigated for a wide number of binary oxide glasses. The usage of Nd^{3+} as structural probe has similar advantages as Eu^{3+} as it also has structurally relevant transitions in the visible range. [9],[10]

Generally speaking, the idea of doping glasses with RE ions is not only based on their suitability as structural probes, but also on their usage as industrially relevant applications, e.g. in solid-state lasers. These optical applications are based on modifications of the energy level structure of the RE dopant ions caused by the glassy host material. Anyway, to meet the technological needs of the respective applications of the RE materials, the optical changes in dependence of the host glass composition must be investigated systematically in terms of fundamental research. [9]

The glasses investigated in the present work belong to the family of binary and ternary sodium borate glasses. However, the focus lies on the ternary glass family consisting of Na_2O, B_2O_3 and Al_2O_3 (NABAL). This ternary glass family has a few advantages compared to its binary equivalent: They feature a higher mechanical stability as well as a higher chemical stability with respect to temperature variations and chemical stability under atmospheric conditions. [11]

The aim of this master's thesis is to provide information about the internal structure of NABAL glasses by luminescence and absorption spectroscopy and to compare, relate, and complete the results and theories with the information provided, on the one hand, by Gresch and Müller-Warmuth [12], who performed NMR studies on the sodium boroaluminate glass family, and on the other hand, by Doweidar *et al.* [13], who investigated the properties of this glass family. Therefore, the influence of the melting time and the composition on the internal structure on the optical spectra of NABAL glasses are investigated. Further, the densities are determined and calculations of the theoretical optical basicity, molar volume, packing ratios and the substructure amount are performed.

II Fundamentals of glasses

1. Definition of the glass state

Glasses can be described as supercooled melts in a rigid state. This state is obtained through congealing. Hence, glasses cannot directly be described by one of the three "classical states" of matter: solid, liquid or gaseous. For a general description of the glass state, on the one hand, one can say that their mechanical properties are defined by the rigidity of crystals and on the other hand, by the disordered structure of liquids. This is confirmed by physical measurements and X-ray diffraction (XRD) studies. Hence, the definition of glasses rather refers to a glassy state, which describes a state "in which the molecular units have a disordered arrangement, but sufficient cohesion to produce overall mechanical rigidity". Thus, glasses are considered as amorphous materials showing a short-range order but no long-range order. Therefore, "vitreous state" is often used as an equivalent term. [14],[15],[16]

The glassy state can be obtained by quenching. This refers to a rapid cooling process of a liquid below the melting point T_m. During this cooling process, the melt is metastable to crystallization, but the formation of crystalline nuclei is a time-consuming process. However, in the cooling process, the molecular motion rapidly slows down and hence, transport processes, which are important for nucleation and crystal growth, are inhibited. Because of this, the crystallization process does not take place and the glassy state is reached. [15],[17]

Figure 1 shows the enthalpy and volume curves for a fast and a slowly cooled glass and for a crystal in dependence of the temperature at constant pressure. In these figures T_m refers to the melting temperature and T_f to a fictive temperature, which is derived from the extrapolations of the supercooled melt and the solid glass lines to their point of intersection. The range between T_m and T_f is called *glass transformation region*. [17]

The glass formation process shows a continuous change of the enthalpy with temperature whereas the crystal formation process shows an abrupt change of enthalpy. When the supercooling process continues further, one can observe an increase of viscosity in the glass transformation region by around 15 orders of magnitude. In this region, the structure of the supercooled melt differs from the structure, which would be present in the case, when there is enough time for the cooling process. Hence, enthalpy and volume are different from the equilibrium values and can be determined by the specific heat or the thermal expansion of the melt. When the viscosity reaches a value where the structure is no longer dependent on the temperature, the configuration of the melt can be described as isoconfigurational or it can be said that a glass is obtained. [17]
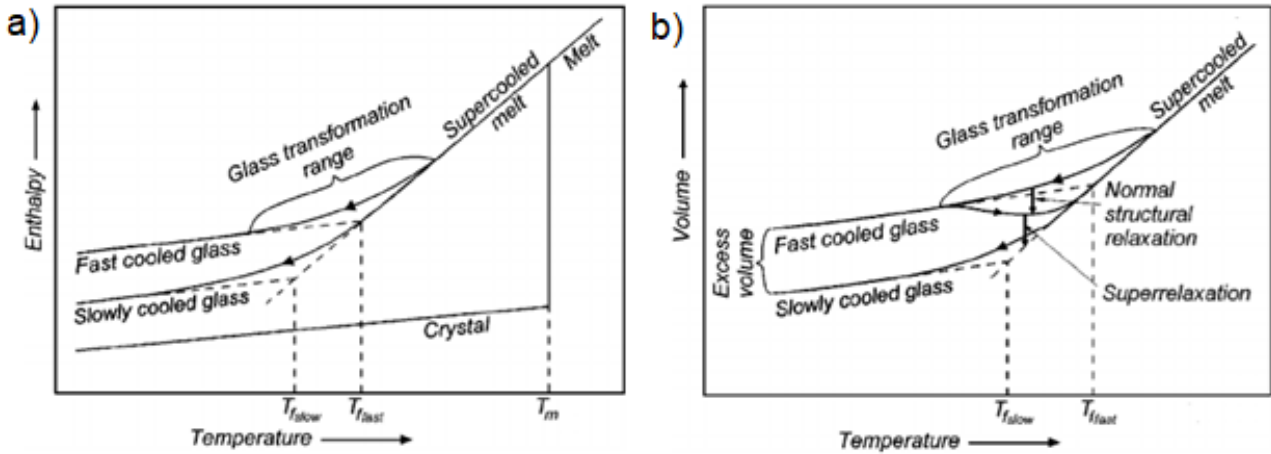
Figure 1 a) Enthalpy and b) volume curves of the glass formation process in dependence of the temperature [17]

2. Glass making in science and technology: A historical overview

The glass making process has a long history whereas its scientific understanding is rather at an early stage. Nevertheless, speaking about the history of glass, one must go back to the formation of the earth. In this event, potstone, perlite and other minerals were congealed to natural glasses in fast cooling processes. Nowadays, glasses can still be formed naturally during volcanic eruptions. [18]

However, the history of human glass making goes back about 4000 years in Mesopotamia. At this time, glass was made from sintered bodies of sand and desert soda with the purpose of creating decorative objects. In order to give colour to these pieces, different salts of copper or manganese were added to the melt. This "material doping" is considered as the first example of the use of minor ingredients to influence the properties of glass. [19]

2000 years later, the glass forming process via pipe blowing was invented, probably in Syria. This newly discovered technique quickly spread across the Roman Empire resulting in a rapid increase in application possibilities of glass products. These developments also led to the demand of a higher quality of the glasses. Thus, efforts were made in the selection process of raw materials resulting in the usage of crystals (quartz) and white stones without coloured inclusions instead of sand to obtain high-quality glasses. The problem was that due to the purification process, not only impurities were lost but also much of the alkaline and aluminium compound, which led to a high moisture sensitivity of the produced material. This is also one of the reasons, why the famous "cristallo" glass, which was made at the beginning of the 16th century in Murano, Venice, shows crizzling on the surface. Because of this, it can be argued that the clarity of the glasses was improved in this period, but a lack of chemical durability was still present. [19]

This changed, when George Ravenscraft invented truly moisture-resistant potash lead glass in England during the 17th century. Hence, the business of lead crystal products grew based on advantages of the new material, e.g. a higher refractive index. [19]

Anyway, it was not before 1800, when glass making for scientific purposes began. The efforts of Fraunhofer, who concentrated on the investigation of glass compositions and glass structure, led to the discovery that chalk and lead containing glasses do have different refractive indices. This event later marked the hour of birth of spectroscopy, optics and glass science. [18]

Apart from the success of the famous physicist Gabriel Stokes, whose investigations led to the design of the first telescopes based on boric and phosphoric acid-based glasses, not many scientific glass experiments ended successfully. Among others, Goethe, made the effort to start a glass melting business in 1829 at the University of Jena to investigate refraction and scattering in strontium glasses. Regardless, these investigations only led to the awareness that not only optical glass properties could be influenced by dopants. [18]

The next event worth-mentioning is the invention of borosilicate glasses leading to the development of better microscopes, telescopes, field glasses and photographic objects. These technological advances where driven by the chemist Otto Schott, physician Ernst Abbe and instrument builder Carl Zeiß in the 19th century. Furthermore, without the work of Abbe and Schott, the discovery of the tuberculosis, cholera and malaria pathogen would never have been possible. [18]

Another popular event in glass history took place in 1936 with the publication of a patent of G.W. Morey, who on the one hand produced glasses of pure B_2O_3 and on the other hand, reduced the B_2O_3 fraction to 10 wt% but added components like lanthanum or tungsten as main compounds. However, these glasses could not make a complete breakthrough because of their low viscosity and their tendency to crystallisation. These properties inhibited the large-scale production of these glasses. Nevertheless, in this era, achievements like complete electric heating systems in connection with a new melting and founding technology were made. Simultaneously to the development of optical glass, progresses were also made in the field of technical glasses. Here, the discovery of glass building properties of boric, phosphoric and silica acid was also crucial. Soon, the precursor of today's Pyrex glass based on borosilicate material was invented, again by Schott. [18]

Nevertheless, the family of binary and ternary borosilicate glasses is already well investigated in literature, whereas the investigation of boroaluminate glasses is rather at an early stage of development. In particular, the field of NABAL glasses remains rather untouched in literature. Therefore, this thesis focuses on basic structural investigations of this glass family.

3. Theories on the glass structure

The first investigations, which can be considered as structural investigations, were carried out by Tamman in 1903. He described the glass formation process as a freezing-in of a liquid-like structure and he also gathered fundamental information about nucleation and crystallization processes. Further relevant knowledge was provided by Goldschmidt in 1926, who postulated that the ratio of the radii of cations and anions must be in the range of 0.2 to 0.4 for network formers like SiO_2 or B_2O_3 to obtain glass. This was later verified by the discovery of the formation of BeF_2 glass. Additionally, Goldschmidt stated that the formation of glass and crystal structure follows the same laws and dependencies. [20]

However, the most ground-breaking theory was provided by Zachariasen in 1932. This theory has its roots in the XRD analysis of crystalline silicates, a work that Bragg and Pauling and their groups began in 1926. [21]

The so-called *random network theory* is based on the awareness that glasses and crystals with similar compositions show similar behaviour. Thus, Zachariasen assumed that the same atomic forces are present in both crystals and glasses leading to the formation of oxygen polyhedral not only in crystals but also in glasses. Further, he embraced the loss of crystalline order due to variations of the A-O-A (A = B, Si, As, Ge, etc.) bond angles resulting in the distortion of the polyhedron. Hence, a random network is obtained. Consequently, one can summarize, that glasses consist of structural units of short-range order randomly linked together to form a network without long-range order. Because of its random structure, glass has a higher internal energy than a crystal which presents the same composition. Only when the difference of the internal energies is small, the glass formation is the favoured process and crystallisation does not occur. To keep this energy difference small, an open and flexible network which is relatively free of distortion is summarized by the four rules of Zachariasen for glass formation of oxide glasses A_mO_n:

1) Oxygen atoms are linked to no more than two A atoms
2) A atoms have a small coordination number (3 or 4)
3) Oxygen polyhedra share corners with each other, neither faces nor edges
4) Minimum three corners are shared

The more rules are fulfilled, the more favoured is the glass formation process. [22],[23],[24]

Figure 2 represents the differences and similarities between crystal and glass structure showing a crystal structure and a glass structure of A_2O_3 with AO_3 triangles as structural units. [25]
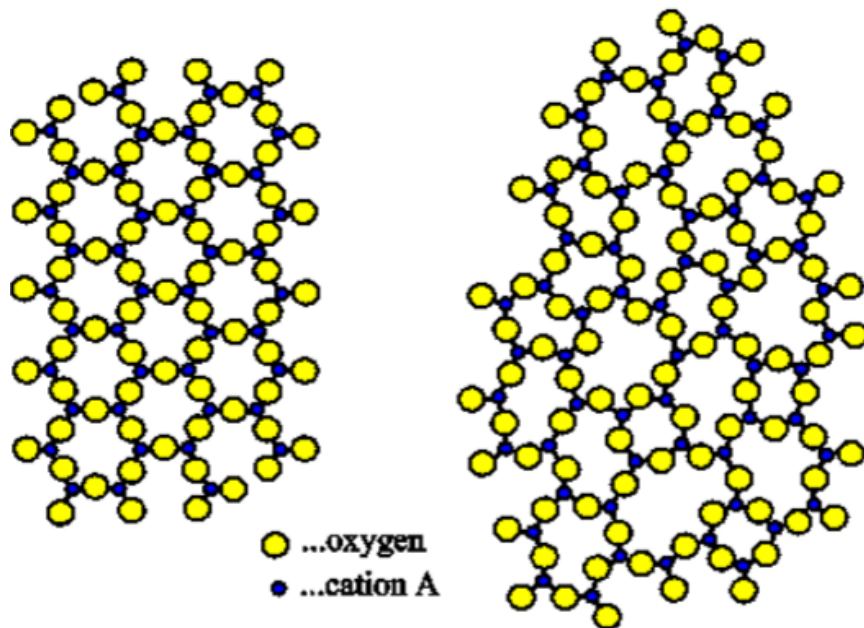
Figure 2 Schematic representation of a crystal structure (left) and a glass structure (right). [25]

4. Network formers, network modifiers and intermediates

In Zachariasen times all known glasses consisted of oxide materials. Zachariasen divided the materials into three categories: network formers (oxides with cations Si, B, P, Ge, As, Be with coordination numbers of 3 or 4), network modifiers (oxides with cations Na, K, Ca, Ba with coordination numbers ≥ 6) and intermediates (e.g. Al_2O_3, PbO). The latter can act as network formers, which are generally cations with a coordination number of 4, or network modifiers, which are generally cations with a coordination number of 6 to 8, depending on the cation's nature of the other oxides in the glass and on the composition of the glass. The intermediates are unable to form a glass per se. [26],[27]

In his work, Zachariasen considered cations as network formers according to his rules in association with oxygen. Together with the oxygen anions, the cations form the random network. When a metal oxide with a cation, which is of the type of a network former, is added to a single component glass, a network containing two different structural units is obtained. Consequentially, one gets a multicomponent glass, which is created by various network formers. In both single and multicomponent glasses, all oxygen anions act as bridging oxygens (BO) between the structural units. Because of this, a three-dimensional network is established. Oxides, which are not directly involved in the network formation, are so-called network modifiers. [27]

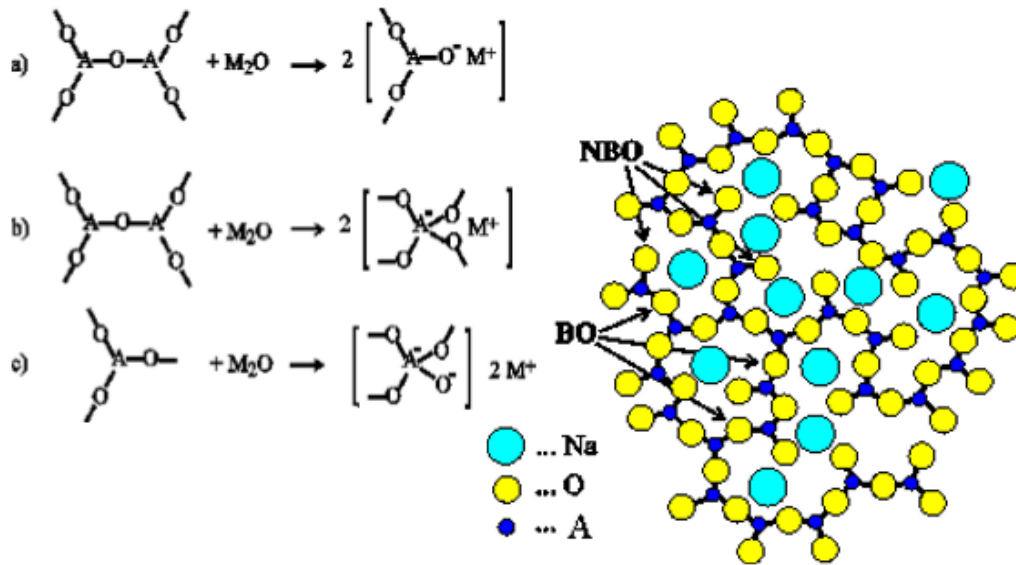In literature, one can find three mechanisms of how they work (*Figure 3*).

Figure 3 Schematic representation of the mechanism possibilities of modifiers M_2O acting in oxide glasses [25]

The first mechanism, represented in *Figure 3 a)*, shows the rupture of the bonds between structural units and hence the creation of non-bridging oxygens (NBO). The network gets loosened, the network connectivity decreases, and its flexibility increases. Another possibility, which is shown in *Figure 3 b)* is that the network modifier increases the coordination number of the network-forming cations. In this way, the connectivity of the network increases, and the flexibility decreases. The third mechanism, represented in *Figure 3* c), shows a combination of both mechanisms. In all the three possibilities, the counterion for the introduced negative charges are the cations of the modifier. [27]

Concerning the behaviour of the intermediate oxygens as network formers or network modifiers, several theories have been proposed in literature. Because of its relevance, only two of them are mentioned here. [27]

Dietzel describes the classification of cations as network formers, network modifiers and intermediates by their respective "electric field strength" (1):

$$F = \frac{Z_C}{a^2} \qquad (1)$$

Z_c represents the valences of the cation and *a* is the sum of the radii of cations and anions. According to Dietzel, network modifiers have a field strength from 0.1 to 0.4, network formers from 1.4 to 2.0, and intermediates from 0.5 to 1.0 The concept of electronegativity by Pauling leads to a similar classification but Dietzel's concept of field strength is applied in a broader way in glass technology. [26],[27]

Sun's so-called single bond strength criterion relates the role of intermediates to the strength of the A-O bonds in A_mO_n oxides. By calculations he found that network formers have bond strengths higher than 380 kcal·mole^{-1}, network modifiers less than 250 kcal·mole^{-1} and intermediates between 250 and 315 kcal·mole^{-1}. The concept of Sun is based on the idea that in the rapid cooling process of the glass formation, the oxides are unable to rearrange bonds when the transformation from the liquid state (melt) to the solid state takes place. [27]

5. Binary alkali borate glasses

Binary alkali borate glasses consist of boron oxide and alkali oxide, whereas the first one acts as network former and the second one as network modifier.

In alkali borate glasses, the modifier may act according to all three possible mechanisms presented in *Figure 3* in dependence of the modifier concentration. Further, borate glasses feature a non-linear dependency of many physical properties like the thermal expansion coefficient and the viscosity. This phenomenon of missing linearity is also called *boron anomaly*. [28],[29]

Krogh-Moe was the first to dedicate investigations on the structure of borate glasses. His analysis was based on IR and X-ray spectra. The proposal of four different possible groupings of the boron and oxygen atoms in the structure of binary borate glasses as a function of the alkali concentration is considered as the culmination of his work. These substructures are stable and well-defined BO_3- and BO_4- subunits, not just randomly linked via corners. The possible subunits are shown in *Figure 4*. [4]

• Boron ions   ○ Oxygen ions
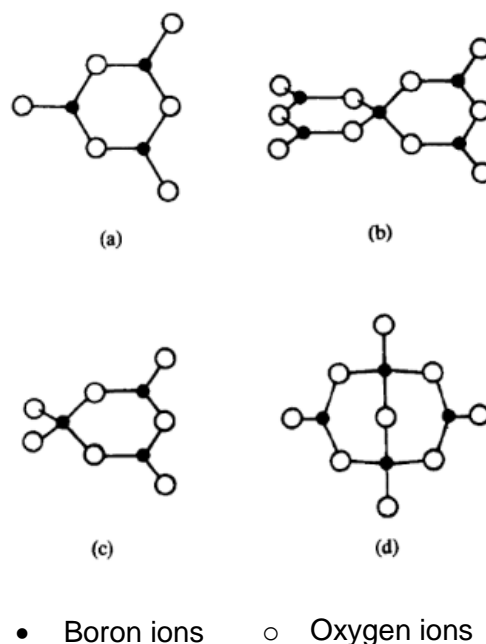
Figure 4 Structural groupings in binary alkali borate glasses proposed by Krogh-Moe
a) boroxol ring b) pentaborate c) triborate and d) diborate groupings [4]

9

Figure 4 shows the formation of *a)* boroxol rings, where the boron atoms are three coordinated ($N_3(B)$), *b)* pentaborate, where the boron atoms are three and four coordinated $N_4(B)$, *c)* triborate, where one boron atom is four coordinated and the others are three coordinated and *d)* diborate groupings, which refer to boron atoms, which are alternated three and four coordinated. The BO_3 units are planar and the BO_4 units are tetrahedral.

The work of Krogh-Moe was later proved by Bray *et al.* via NMR studies and by Konijnendijk via Raman spectroscopy. [30]

The dependence of the formation of these groups on the alkali oxide concentration proposed by Krogh-Moe is shown by the dashed lines in *Figure 5*. The solid line represents the experimental results from NMR data. The tetraborate groupings are a mixture of pentaborate and triborate groupings. [30],[31]
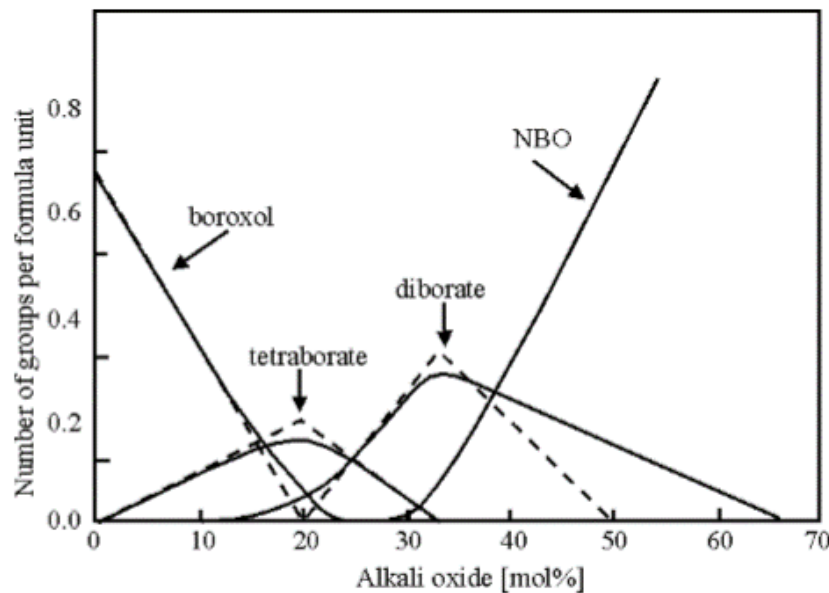

Figure 5 Structural model of binary alkali borate glasses: The solid lines represent the experimental results and the dashed lines the predicted model of Krogh-Moe. [25]

Figure 5 shows that without any modifier, the glass consists of approximately 75 % boroxol rings. With increasing modifier concentration, the number of tetraborate groupings increases. These groupings are converted to diborate groupings. At about 25-30 mol% alkali oxide concentration all boroxol rings disappear and the formation of NBOs increases rapidly.

The diborate groupings contain the most BO_4 units. Therefore, based on the work of Krogh-Moe and the experimental results, at about 33 mol% the most BO_4 units are present. It was shown by Bray *et al.* that the $N_4(B)$ increases up to 45 mol% for various alkali metals (Na, K, Li) and decreases until an alkali concentration of ~ 70 mol%. (*Figure 6*). [25],[32]
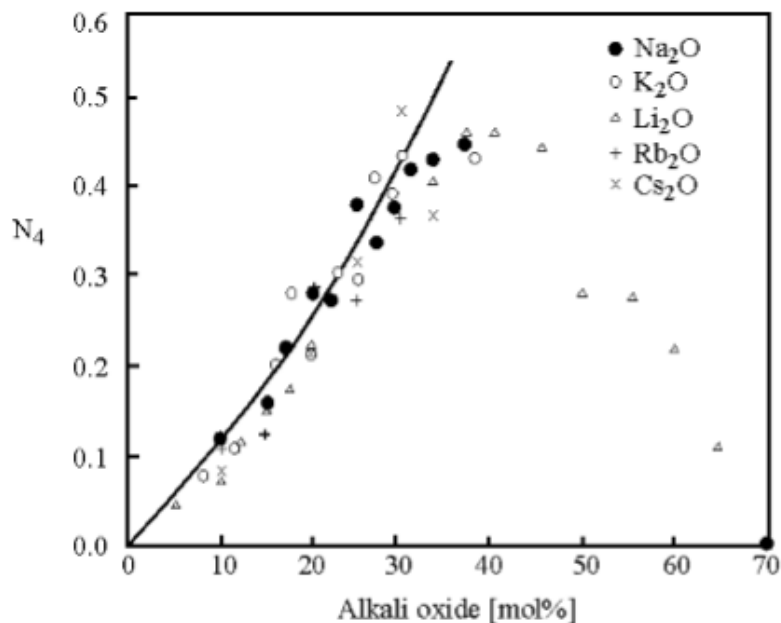
*Figure 6 Fraction N₄(B) in binary alkali borate glasses as a function
of the alkali concentration in mol% [32]*

It was tried to relate the boron anomaly with the structural changes in the glasses. This was first not possible because according to Gooding [33], the thermal expansion coefficient shows a minimum at about 16 mol% Na_2O. This is correlated with the viscosity, which shows a maximum at these percentage. Biscoe and Warren related those property changes with changes in coordination of boron and the number of NBOs. When NMR investigations were possible and the data represented in *Figure 5* and *Figure 6* were published, it was obvious that the data do not affirm the theory of Biscoe and Warren [34]. In response to this disagreement, Uhlmann and Shaw [35] reinvestigated the thermal expansion coefficient in binary sodium borate glasses and concluded that the pronounced minimum at 16 mol% modifier content does not exist, but the thermal expansion coefficient decreases slowly up to 30 mol% Na_2O. Therefore, it could be assumed that the changes of properties are related to the compositional changes corresponding to the relative amounts of the structural groupings.

6. NABAL glasses

The term "NABAL Glasses" describes the ternary glass family consisting of Na_2O, B_2O_3 and Al_2O_3. Na_2O and B_2O_3 play the same role as in the binary glass systems, which is network modifier for the alkali oxide and network former for the boron oxide. Al_2O_3 can act both as a network former and as a network modifier.

Gresch and Müller-Warmuth [12] investigated the structure of NABAL glasses in dependence of the composition via ^{11}B and ^{27}Al NMR spectroscopy. It was disclosed that the alkali oxide Na_2O associates with both B_2O_3 and Al_2O_3 to form N₄(B) and tetrahedrally coordinated

aluminium, denoted as $N_4(Al)$. The number of $N_4(B)$ shows a linear dependence for $Na_2 \leq 30$ mol% with increasing R (Na_2O concentration in mol% divided by the B_2O_3 concentration in mol%) values and can be described by (2). [36],[37]

$$N_4(B) = \left(1 - 0.031 y_{Al_2O_3}\right)R \tag{2}$$

$y_{Al_2O_3}$ is the molfraction of Al_2O_3 in mol%. *Formula* (2) is limited by $N_4(B) = R$ for zero aluminium concentration. For Na_2O contents higher than 30 mol%, *Formula* (2) leads to values higher than observed. As it arises from *Formula* (2), the slope of this correlation is determined by the Al_2O_3 concentration of the glass. For smaller Al_2O_3 concentrations, the increase appears more sharply than for higher Al_2O_3 concentrations. The systematic decrease of the slopes with an increasing Al_2O_3 concentration shows that not all oxygen ions from Na_2O, which form part of BO_3 units are then changed to form part of BO_4 units. This occurs because part of the oxygen ions is now needed for the four-coordination of aluminium atoms. At higher Al_2O_3 concentrations, the less drastic decrease in $N_4(B)$ can be explained by the fact that Al_2O_3 may serve as a solvent for the BO_4 tetrahedral network, of course also containing AlO_4 units. The aluminium partially suppresses the formation of NBOs. The competition of the formation of four-coordinated aluminium and boron can be described by the following reaction equations: [36]

$$B_2O_3 + Na_2O \rightarrow 2\,BO_{4/2}^- + 2\,Na^+$$
$$Al_2O_3 + Na_2O \rightarrow 2\,AlO_{4/2}^- + 2\,Na^+$$
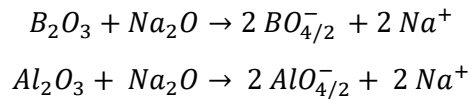
Each oxygen ion will be shared by two tetrahedra (dicluster). The generated Na^+ ions are then located in network interstitals and stabilize the tetrahedra. As there is a decrease of $N_4(B)$, with increasing concentration of Al_2O_3, one can assume that the second reaction is favoured. This means, that the necessary Na_2O amount is first consumed for the formation of four-coordinated aluminium and the rest for the formation of four-coordinated boron. For low sodium oxide content, oxygen is missing and therefore triclusters consisting of three tetrahedral AlO_4 and/or BO_4 units sharing one oxygen atom are more probable than simple AlO_4 tetrahedra. Based on these assumptions and the experimental results which led to *Formula* (1) the number of four-coordinated alumina is direct proportional to the mole fraction of sodium oxide. This can be described by *Formula* (3): [36],[37],[38]

$$N_4(Al) = 0.031 x_{Na_2O} \tag{3}$$

As *Formula* (3) is directly related to *Formula* (2), it is also only valid for Na_2O contents up to 30 mol%. *Formula* (2) implies that, for Na_2O concentrations greater than 30 mol%, practically all aluminium atoms are four-coordinated. The remainder or "excess" of the aluminium atoms, which cannot coordinate tetrahedrally anymore, increases with decreasing Na_2O concentration. Aluminium is unable to form triangular units. Gresch and Müller-Warmuth refer in their work to former investigations of Lacy (1963) and Waal (1969), who suggested that this remainder could be held in six-coordination or alternatively in network interstitials. The first theory was already proved for CaO-B_2O_3-Al_2O_3 (CABAL) glasses indicating the transformation from AlO_6 to AlO_4 units. [12] Doweidar *et al.* assumed that aluminium forms AlO_6 units. [37]

To sum up, one can say that the aluminium coordination rarely varies with oxygen availability, but the different interlinking of AlO_4, BO_4 and BO_3 units in the network undergoes severe changes. However, the situation is complex due to the simultaneous use of oxygen for the formation of both AlO_4 in diclusters and triclusters and further, because also a fraction of the BO_4 groups could be included in the triclusters. Moreover, for high Na_2O contents, also some triclusters may occure. The excess oxygens are then left as NBOs. [36]

In 1986 Zhong and Bray dedicated further investigations to the structure of NABAL glasses. They found out that between R values of about 0.3 to about 0.7, the substructure amount of three-coordinated boron without any NBOs decreases whereas between R values of about 0.3 to 0.6 the substructure amount of three-coordinated boron with one NBO is continuously on the increase until it starts to decrease at 0.6. Also, the substructure amount of three coordinated boron with two NBOs is on the increase between $R = 0.5$ to 0.7. Further, binary and ternary glasses of the NABAL family were compared showing an increase of $N_4(B)$ for sodium borate glasses with R between 0.18 and 1.14 and a decrease of $N_4(B)$ for the ternary system between 0.4 and 0.7. [38]

Doweidar *et al.* [37] studied the properties structure correlation of NABAL glasses and found out that significant changes in the density ρ, the glass transition temperature T_g and the thermal coefficient α above 15 mol% Al_2O_3 occur due to the formation of triclusters. The increase in the fraction $N_3(B)$ with increasing aluminium oxide content up to 15 mol% should be related to the decrease in ρ. [37]

III Rare Earth Ions as structural probes in glasses

1. Rare earth ions: Classification and properties

RE elements embrace yttrium, scandium, and the lanthanide series from lanthanum to lutetium. All RE elements except for promethium, which was the last to be found in 1947, were discovered within a bit more than a century starting in the late 18th to the beginning of the 20th century. Generally speaking, RE elements are of interest because of their unique optical properties (*see III 3. Spectroscopic fundamentals of rare earth doped glasses*). [39]

Basically, there are two reasons for the denomination "rare earth elements". First, they have a low abundance in nature. Nevertheless, one must point out, that, e.g. cerium still has a higher deposit than lead, mercury or cadmium. Hence, it must be distinguished between lanthanides with even atomic numbers, which show a considerably higher occurrence in the earth crust (10^{-3} to 10^{-4} wt%) from those with odd atomic numbers (10^{-4} to 10^{-5} wt%). Concerning their mode of deposit, RE elements are not incorporated into petrogenetic materials because of their larger atomic radii compared to those of most of the trivalent metal ions. Therefore, they form minerals with elements featuring similar atomic radii, for instance Eu^{2+} (117 pm) and Sr^{2+} (118 pm) in strontianite $SrCO_3$. Secondly, they are complicated to extract and to separate from each other. [39],[40]

The properties of the elements of the lanthanide series are very similar, as they only differ in the filling of the f-shell, which is well shielded by filled outer electron shells. All lanthanides exist in the crystal structure of close packaging, except for samarium and europium, which show a body-centred cubic crystal structure. The densities, melting points and sublimation enthalpies of europium and ytterbium feature minima whereas their atomic radii feature maxima in the lanthanide series. In their metallic state lanthanide atoms normally contribute three electrons to the electron gas, except for europium and ytterbium, which only contribute two electrons leading to very stable f^7- and f^{14}-configurations. The smaller attraction between the electron gas and the metal ions in these elements lead to their exceptional properties. Concerning the atomic radii of the trivalent lanthanide ions, the radii decrease with increasing atomic number due to the lanthanoid contraction. [40]

2. Rare earth ions in glasses: Modes of incorporation

RE ions dissolve in glasses as structural units. To be more specific, one can find four different possibilities of incorporation of RE ions into glasses, which are all based on the understanding of glass as a solvent and thus, on dissolved ions in a glass melt.

Figure 7 shows a scheme of the four different modes of incorporation: 1) *Molecular complexes*, 2) *Quasi-molecular complexes*, 3) *Network modifiers* and 4) *Network formers*. [41],[42] The different modes are described below *Figure 7*.
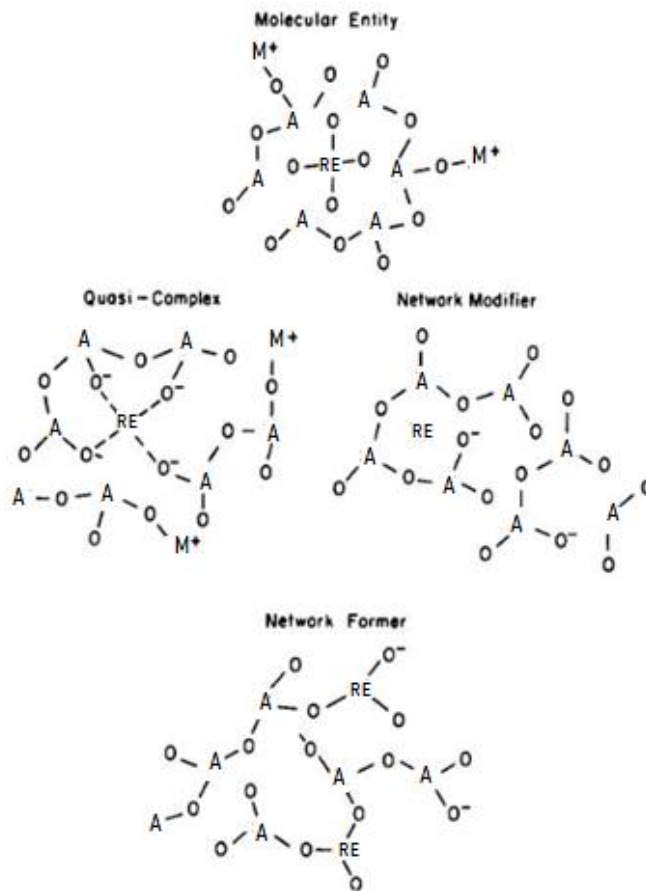

Figure 7 Schematic representation of the modes of incorporation of RE ions into a glass network, adopted from reference [41]

1) *Molecular complexes*

The RE ion is coordinated to four oxygen atoms not forming part of the network.

2) *Quasi-molecular complex*

The RE ion is coordinated by NBOs. This mode of incorporation may result in local geometrical rearrangement of the surrounding glass-forming network to fulfil the bonding requirements. Hence, the bond lengths are adjusted leading to a more regular coordination polyhedron.

3) *Network modifier*

The RE ion simply occupies a normal vacant site and creates NBOs in its neighbourhood.

4) *Network former*

The RE ion is incorporated into the network either by substitution of sites or by polymerization of the tetrahedral. [41],[42]

According to the investigations of Neuhold [43] it is impossible to dissolve Eu_2O_3 in the glass melt at too little modifier concentrations or even without any modifier. Additionally, it could be excluded that Eu_2O_3 acts as modifier itself, as it was not possible to obtain a transparent glass containing only B_2O_3 as a network former and Eu_2O_3 as the modifier/dopant compound. Further, Eu_2O_3 can only act as a network former at concentrations considerably higher than those used for the glasses prepared in this thesis. The presence of the RE dopant as molecular complexes is only expected to occur for small, highly charged ions such as Cr^{6+}, Mo^{6+} or W^{6+}. Hence, quasi-molecular complexes surrounded by NBOs result to be the most probable for Eu^{2+}/Eu^{3+} and Nd^{3+} ions. The exact formation of the coordination polyhedra depends upon the balance between the bonding properties of the ion and on the network bonding strength. [41],[42]

3. Spectroscopic fundamentals of rare earth doped glasses

3.1. Term symbols [44],[45]

For the description of the energy levels of atoms or ions with more than one electron, the Russell-Saunders coupling scheme is used for light atoms and the jj-coupling is used for atoms heavier than bromine. Nevertheless, the Russell-Saunders coupling scheme is used in RE spectroscopy to describe the states and transitions in RE ions but with the restriction that, in fact only the value of J is a "good" quantum number.

The Russell-Saunders term symbols consist of three constituent parts (*Figure 8*):
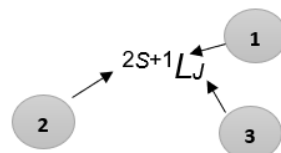
Figure 8 Illustration of Russel-Saunders term symbols with
1 total orbital angular momentum quantum number, 2 spin multiplicity
and 3 total angular momentum (orbital and spin) quantum number

(1) **L** is the *total orbital angular momentum quantum number*, which is derived from the combination of the orbital angular momenta of the individual electrons in the ion in accordance with the Clebsch-Gordan series.

(2) The term **2S+1** refers to the *spin multiplicity* of the term, which describes the number of possible orientations of the overall spin of the ion. *S* is the total Spin of the ion.

(3) **J** is the *total angular momentum (orbital and spin) quantum number* and is determined by the Russell-Saunders coupling scheme.

3.2. Properties of rare earth ions in host materials

A RE ion in a glass can be considered as an impurity in small quantities in a host material. Because of this, optically active centres are formed, which emit luminescence in the case of excitation. The host materials have a great influence on the spectra of the "impurity ions" resulting in the ligand field theory or, in case of an ordered periodic lattice, in the crystal field theory. [46]

Figure 9 shows a visual representation of the RE ion atomic structure surrounded by its host material.
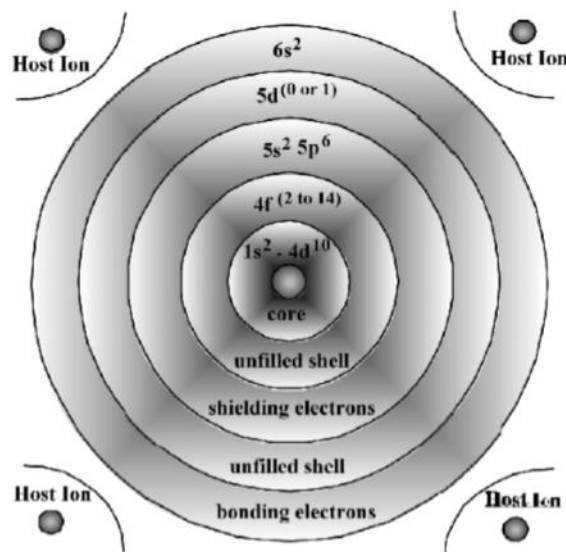
Figure 9 Atomic structure of a RE ion [46]

All lanthanide ions have a Xe-core, an unfilled f-shell and some outer shells that shield the 4f-shell from influences of the host material and from further influences of the surrounding field leading to the characteristic sharp and well-defined band spectra, which are quite similar to those of their free ions. Though, like mentioned above, lanthanide ions experience a weak external field. The free ion $^{2S+1}$J states splits into $^{2S+1}$L$_J$ multiplets represented in the spectra. [46]

In host materials, like crystals and glasses, RE ions are usually incorporated as divalent or trivalent cations showing different spectroscopic behaviour. When a trivalent RE ion is formed, 5d-, 6s- and some 4f-electrons are removed. Hence, transitions between electronic energy sublevels of the $4f^n$-configuration take place. Divalent RE ions contain one more f-electron. In contrast to its trivalent equivalents, they preferably show f → d interconfigurational transitions. [47],[48]

For this thesis the RE elements europium and neodymium are of interest because of their unique optical properties and further, because their usage as structural probes in host materials is widely spread in literature. *Table 1* presents the electron configurations of the RE atoms and its trivalent ions.

Europium		Neodymium	
Eu	$[Xe]4f^75s^25p^66s^2$	Nd	$[Xe]4f^45s^25p^66s^2$
Eu^{3+}	$[Xe]4f^65s^25p^6$	Nd^{3+}	$[Xe]4f^35s^25p^6$

To be more specific, the trivalent europium ion is of utmost importance in this work, although some of the recorded spectra also proof the presence of the divalent europium ion. The general electron configuration of europium is $[Xe]4f^75s^25p^66s^2$. 5s- and 5p-electrons, of course, are part of the [Xe] configuration but are mentioned here explicitly to highlight that the f-shell is an inner shell. The electron configuration of the trivalent ion is $[Xe]4f^65s^25p^6$. As in all lanthanoids, the 4f-electrons are well shielded by the 5s- and 5p-outer shells and hence, they are only weakly affected by the ligands leading to narrow bands in the spectra. [47]

Nevertheless, there are several interactions within the f-shell of the Eu^{3+} ion, leading to the actual lifting of the $4f^6$-configuration: Firstly, electron repulsion caused by the electrostatic interactions between the electrons in the 4f-shell has an influence on the degeneracy. Further, the spin-orbit coupling, which has its roots in interactions between the spin magnetic moment of the orbital angular momentum of electrons and the magnetic field of the electron moving around the nucleus. Also, despite the location of the 4f-shell as an inner shell, crystal-field effects perturbate the ion, caused by the interactions of the 4f-electrons and the electrons of the host material. [48]

The divalent europium ion has an outer electron configuration of $[Xe]4f^75s^25p^6$. The excited configuration of the divalent ion is close in energy to the $4f^n$ fundamental configuration. Hence, $4f^{n-1}5d^1 \rightarrow 4f^n$ transitions may occur and lead to intense parity-allowed transitions and broad absorption and emission bands. This d-shell is an outer shell and is therefore sensitive to the surrounding and therefore it is highly split due to the crystal field of the ligands as it can be seen in *Figure 10*. This splitting leads to broad bands for the Eu^{2+} ion emission/absorption. Together with Tb^{3+}, Eu^{3+} and Eu^{2+} are commonly applied in the fabrication process of phosphors for red, green and blue lamps. [47]
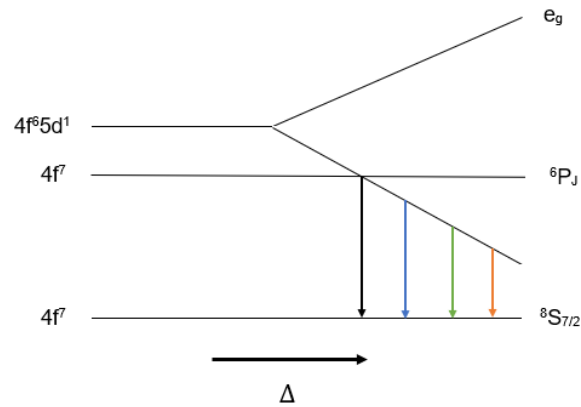
The general electronic configuration of the element neodymium is [Xe]$4f^4 5s^2 5p^6 6s^2$. The electron configuration of the trivalent neodymium ion is [Xe]$4f^3 5s^2 5p^6$. Again, the 4f-electrons are well shielded by the electrons of the $5s^2 5p^6$ less electronic configurations. Analogous to the trivalent europium ion, still several perturbations take place. Nd^{3+} is the most frequently used ion in solid state lasers as it shows several groups of sharp optical transition bands. [49]

The crystal field plays an important role in the Stark effect leading to the splitting of energy levels of ions in host materials. The ligand or crystal field is external to the dopant ion. Its symmetry is determined by the chemical composition of the host material. The dopant ion gets influenced by the electrons of the host material as a repulsive force and by the nuclei as an attractive force. The sum of these interactions results in a net electric field. In the case of the lanthanide dopant ions, the crystal/ligand field is small compared to spin-orbit interactions. In the case of transition metal dopant ions, the situation is reversed. [46]

3.3. Dieke diagram

The Dieke diagram (*Figure 11*) provides an energy level diagram, which is based on the spectra of trivalent RE ions in crystals based on optical measurements in a lanthanum chloride (LaCl$_3$) host. The spectra were provided by Dieke *et al.* in 1968. The width of each state refers to the crystal field splitting magnitude. The energy levels differ slightly when they are incorporated into other crystals. Nevertheless, the gross features of the energy levels remain basically unchanged. [50]
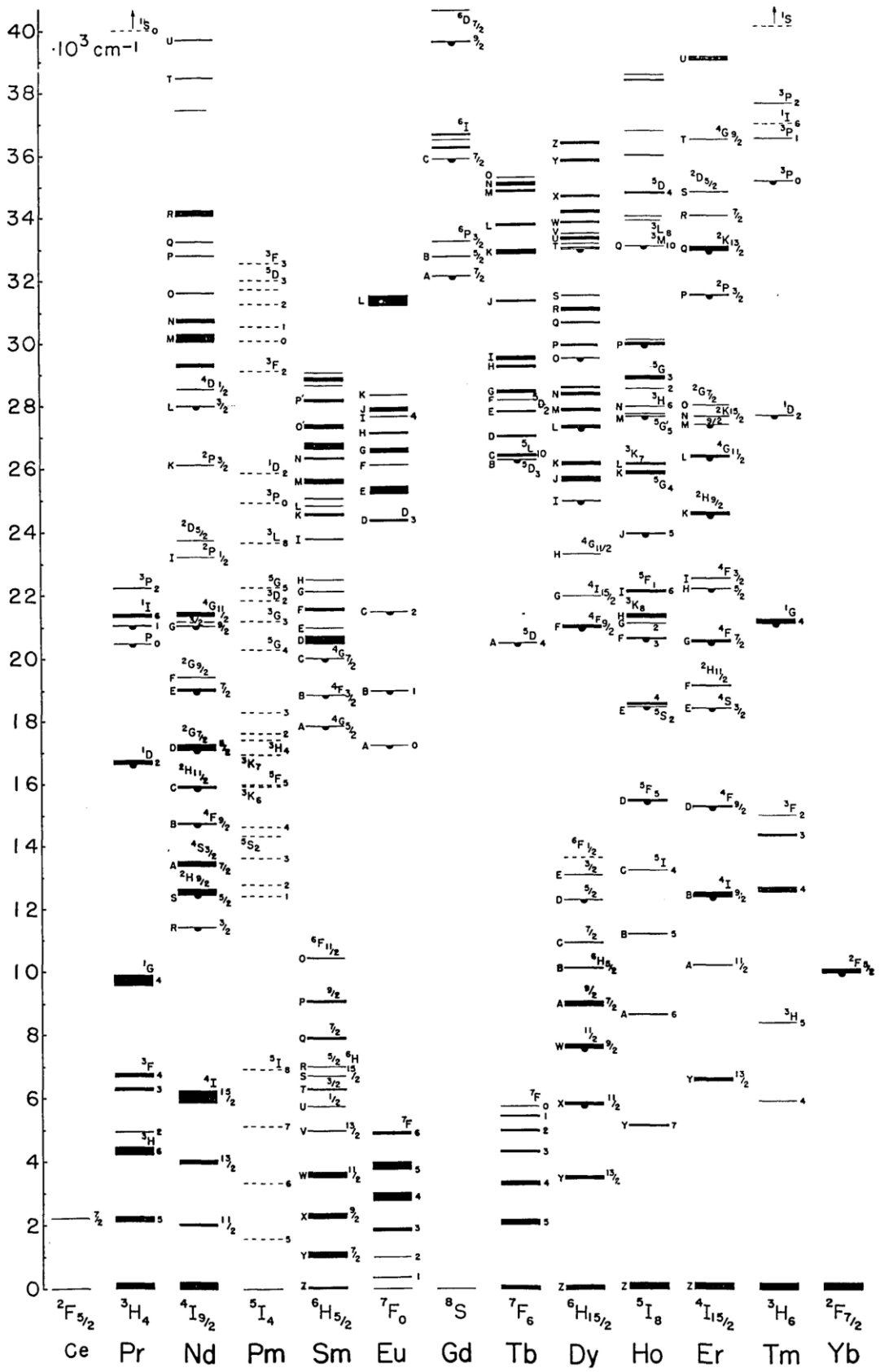
Figure 11 Dieke Diagram, taken from reference [51]

20

Figure 12 shows the magnified free energy level diagrams of the trivalent neodymium and europium ions, as these are the ions relevant for this thesis.

Figure 12 Magnification of the free ion energy levels of trivalent a) neodymium and b) europium ions; adopted from reference [52]

3.4. Hypersensitivity

The phenomenon of hypersensitivity was described by Judd and Jørgensen [53] and highlights the sensitivity of f-f transitions to the symmetry and nature of the host matrix in the low energy region (570-710 nm). This range is characterized by ligand coordination properties as well as the symmetry of the environment, polarizability of the ligands, crystal field strength, etc. Hypersensitivity occurs only when the RE ion is not a centre of conversion. Thus, already small distortions from the inversion symmetry lead to an increase of intensity, whereas other transitions are not notably affected.

For the Eu^{3+} ion, it can be ascribed to the $^7F_0 \rightarrow {}^5D_2$ transition in the absorption spectrum and $^5D_0 \rightarrow {}^7F_2$ in the emission spectrum. [54],[55] For the Nd^{3+} ion, the hypersensitive transition is described by the $^4I_{9/2} \rightarrow {}^4G_{5/2}$ transition. This transition is located next to the $^4I_{9/2} \rightarrow {}^4G_{7/2}$ transition. The band structure of these transitions is determined by two main peaks including also smaller features on their low energy sides. Because of the similarity of the energy of the target states, it is impossible to clearly relate the features to either one of the two manifolds. [56]

Optical investigations of RE ions in solutions with different solvents have displayed that similar environments of the first coordination sphere of the ions lead to similar shapes of the hypersensitive transitions. The band shape is defined by the type (bridging or non-bridging), the number, and the arrangement of the oxygen atoms. Structural information is provided by the changes of intensities and shapes of the sample ions spectra. [56]

For Eu^{3+} doped glasses, the ratio of the electric-allowed dipole transition (ED) $^5D_0 \rightarrow {}^7F_2$ and the magnetic-allowed dipole transition (MD) $^5D_0 \rightarrow {}^7F_1$ is a measure for the degree of distortion from inversion symmetry of the surrounding of the RE dopant ion. This ratio is also called asymmetry ratio (AS). The ED is magnetic-forbidden and electric-allowed in odd field. Hence, this band shows a strong site dependence, whereas the MD $^5D_0 \rightarrow {}^7F_1$ dipole transition does not depend strongly on the site. [57]

3.5. Nephelauxetic effect

The nephelauxetic effect occurs in complexes with transition metals and lanthanides and describes the shift of optical transitions towards lower energy, which occurs due to an expansion of the partly filled electron (f-/d-) shell (for lanthanides/transition metals) towards the surrounding ligands because of attempted covalent bond formation. This leads to a decrease of the electron-electron interaction within the shell. [58]

In optical spectra, a large shift means a large nephelauxetic effect and hence a more covalent character of the bond between an ion and its ligands. Further, in oxide glasses the nephelauxetic series is a measure for the basicity (electron donation) of the metal-oxygen bond. In the case of RE ions the nephelauxetic effect is smaller than for transition metals as their f-shell is an inner shell and hence it is shielded from its surrounding by the 5s- and 5p-shells. The shifts observed for RE ions are only in the order of a few 100 cm^{-1} compared with the free ion. Due to the influence of crystal field splitting, which may occur, singlet to singlet (J = 0) transitions are preferred for the nephelauxetic investigations. [59],[60]

In this thesis, the nephelauxetic effect for Eu^{3+} doped glasses is represented by the $^7F_0 \rightarrow {}^5D_0$ transition and for the Nd^{3+} glasses by the $^4I_{9/2} \rightarrow {}^2P_{1/2}$ transition of the absorbance spectra. The $^2P_{1/2}$ multiplet is preferred, because for RE ions with an odd number of electrons (i.e. Kramers ions) the crystal field in general produces (J + ½) crystal field states. Consequently, the $^2P_{1/2}$ multiplet remains unsplit. [59],[60]

As the covalent character of bonds in a material correlates with the density of bodies, the molar volume, V_m, of the glasses is of utmost importance. V_m is defined by *Formula* (4).

$$V_m = \frac{M}{\rho} \tag{4}$$

With M describing the molecular mass matching with the glass composition and ρ representing the experimentally determined density. Thus, band shifts towards smaller energies correspond to an increasing Nd/Eu-O covalency and an increasing nephelauxetic effect and hence, increasing densities reduce the average Nd/Eu-O distances. [60],[61]

In this work, the position and FWHM of the bands are of interest.

3.6. Optical spectra and relevant transitions of Nd^{3+} and Eu^{3+}

In this part of the thesis, the emission and absorption spectra of both Eu^{3+} doped glasses and the absorbance spectrum of Nd^{3+} doped glasses are shown to give an overview on the relevant bands of the spectra. All the spectra were arbitrarily chosen from the pool of the recorded spectra of the produced glass samples.

Figure 13 shows a typical absorbance spectrum of the Kramers ion, Nd^{3+}, doped into glasses.
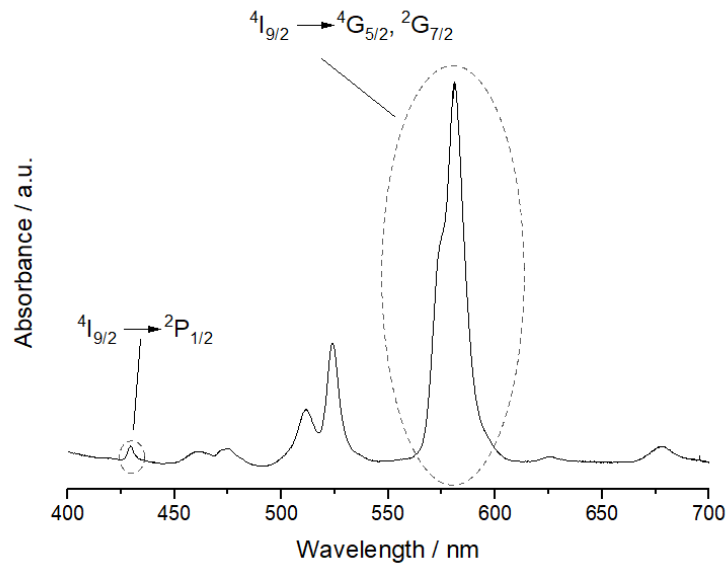
Figure 13 Absorbance spectrum of Nd^{3+} in glass matrix

One can see several groups of relatively sharp optical absorption bands. It consists of transitions between the ground state manifold $^4I_{9/2}$ and several excited states. All transitions are crystal field split by the influence of the oxygens from the immediate environment of the RE ion. The transition $^4I_{9/2} \rightarrow {}^4G_{5/2}$ marks the hypersensitive transition of Nd^{3+} in the host matrix and $^4I_{9/2} \rightarrow {}^2P_{1/2}$ marks the transition used to monitor the nephelauxetic effect. The latter can be described as the so called hotband system of Nd^{3+}. This means that also transitions from the first few excited states of the crystal field split $^4I_{9/2}$ ground state multiplet take place because these are located only a few 100 cm^{-1} above the lowest crystal field component. Hence, transitions from the five (because J = 9/2; so, the number of crystal field states is 5) crystal

field split levels are possible. The occurrence of the bands is temperature dependent: With higher temperatures more bands are visible. [62]

Figure 14 shows the emission spectra of Eu^{2+} and Eu^{3+}.
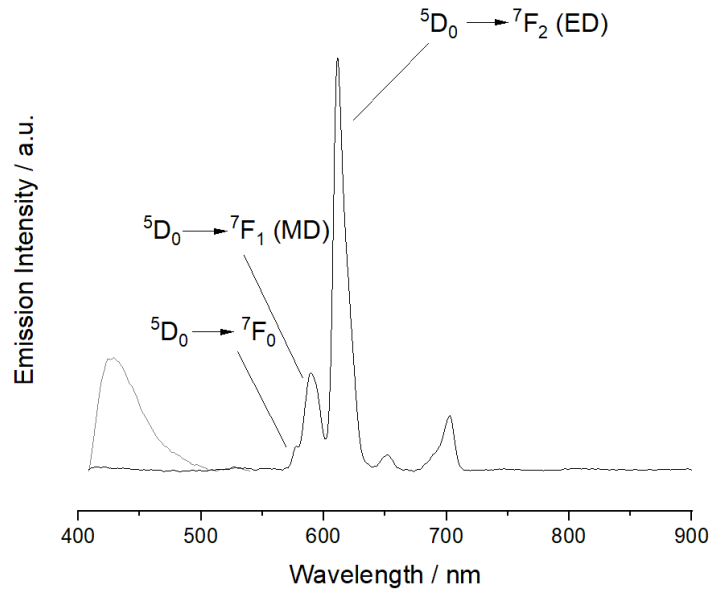
Figure 14 Emission spectra of Eu²⁺ (grey line) and of Eu³⁺ (black line) in glass matrix obtained after an excitation at 394 nm

In the emission spectra of Eu^{3+} the positions of the transition $^5D_0 \rightarrow {}^7F_0$ refers to the nephelauxetic effect. It is located between 570 and 585 nm and it is an induced magnetic dipole transition. This transition is only observed in C_n, C_{nv} and C_S symmetry. The $^5D_0 \rightarrow {}^7F_2$ transition is hypersensitive and is also described as ED. In contrast to this, the $^5D_0 \rightarrow {}^7F_1$ transition describes the MD, as already mentioned in chapter *III 3.4 Hypersensitivity.* [63],[64],[65],[66] Both the Eu^{3+} and the Eu^{2+} ions emit in the visible range when they get excited at a certain wavelength. In the present glasses, Eu^{3+} shows a red emission, whereas Eu^{2+} shows a pink emission. In the emission spectra, one finds the emission band of Eu^{2+} as a broad band located between 350 and 500 nm. The Eu^{3+} ion shows more narrow emission bands around 600 nm. Nevertheless, these bands are inhomogeneously broadened due to the host material. [67] Another aspect worth mentioning concerning the differences of Eu^{3+} and Eu^{2+} are the different decay times of the emission of the ions. This is related to the parity allowed transition of the excited state in Eu^{2+} to the ground state, which has a shorter lifetime than the excited state from the parity forbidden transition of Eu^{3+}. [68]

Figure 15 shows the absorbance spectrum of Eu^{3+}.
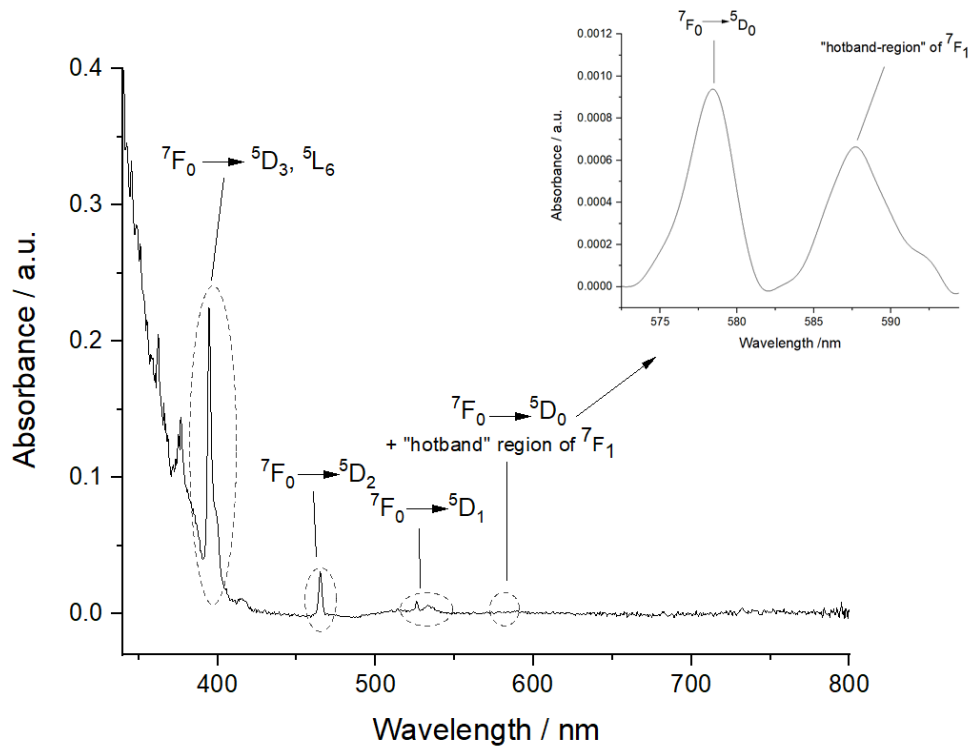
Figure 15 Absorbance spectrum of Eu³⁺ in glass matrix with a magnification of the $^7F_0 \rightarrow {}^5D_0$ transition and the hotband region of $^7F_1$

The $^7F_0 \rightarrow {}^5D_0$ transition refers to the nephelauxetic effect. This transition is electric and magnetic dipole forbidden. Normally, this band represents one of the weakest features in the spectra or does not even show up as in the overview spectrum in *Figure 15*. It can only be seen in the magnified scale in the insert. Further, also excitation from the first excited multiplets $^7F_1$, which is located about 300 cm^{-1} above the ground state and therefore, it is also occupied at room temperature. These so called "hot bands" get more intense with increasing temperature. [69],[70]

The emission spectra of Eu³⁺ (materials) provide more information than the absorption spectra of Eu³⁺ and show intense emission from the $^5D_0$ excited state to the J (J = 0-6) levels of the ground term ^7F. The transitions to the $^7F_5$ and $^7F_6$ levels usually do not appear because they are located outside the detection range of the UV-VIS spectrometers in the NIR. Emission from the higher excited states $^5D_1$, $^5D_2$, $^5D_3$ happen less frequently and have a very low intensity. Most of the transitions the luminescence spectrum shows are induced electric dipole (ED) transitions. ED transitions result from the interaction of the RE ion with the electric field vector through an electric dipole. [67]

3.7. Inhomogeneous broadening

The spectra of RE ions incorporated into amorphous solids show increased widths of bands compared to single crystalline materials due to site-to-site variations of the RE environments. This means that the immediate environment, thus the micro-symmetry around the RE ion, is slightly different from site to site leading to *inhomogeneous broadening* of the bands. [71],[72] Therefore, the FWHM of a singlet to singlet transition is a measure for the variety of the environment of the sites for the RE ions. Smaller site-distributions correspond to smaller FWHM and vice versa. In the present work, the FWHM of the $^4I_{9/2} \rightarrow\, ^2P_{1/2}$ transition in Nd^{3+} doped samples is used to gather information about the site distribution in dependence of the glass composition. [73]

IV Experimental

1. Glass preparation process

The glass making process on a laboratory scale follows some general steps, which are subsequently carried out.

First, the glass components (oxides, carbonates) including the RE oxide are weighted and then mixed thoroughly in a glass mortar for 5 minutes (min). Then, the mixture is transferred to a crucible at an elevated temperature. This is performed stepwise because of the evolution of gases (mainly CO_2 due to $Na_2CO_3 \rightarrow Na_2O + CO_2$). In case of too much simultaneous gas formation, the partially melted powder could rise in the crucible and could further overflow and lead to a material loss. In the next step, the heat treatment continues up to 1200 °C for longer time to complete the melting. The exact temperature programme is shown in *Table 2.* 30 min before the end of the preset melting time, the crucible is swirled to remove existing bubbles in the glass and to ensure the homogeneity of the glass sample. Then, the melt is quenched in a copper mold or on a cold plate. The last step is the subsequent thermal treatment. For this, all the samples are immediately transferred to an oven at temperatures between 430 and 500 °C and cooled down to 30 °C at a cooling rate of 30 °C per hour (h).

For both the heat treatment and the subsequent relaxation treatment *Nabertherm L5/R 1990* ovens were used. For the production of the glass samples, analytical reagents Na_2CO_3 (99.9%, Merck), B_2O_3 (99.8%, Roth), Al_2O_3 (Fluka), Eu_2O_3 (99.99%, Johnson Matthey GmbH Alfa Products) and Nd_2O_3 (99.9% Johnson Matthey GmbH) were used.

As this work is based on the existing literature of the structure of NABAL glasses, a temperature of 1200 °C was chosen because this was also the temperature for the preparation of the glasses in the work of Gresch and Müller-Warmuth [12]. Also, the parameters of the subsequent heat treatment are based on their work. Hence, the results obtained by the NMR studies by Gresch and Müller-Warmuth and the results based on the spectroscopic investigations of this thesis, can be compared.

To proof the influence of the melting time, an additional series was prepared. It was found out, that the melting time does not have any significant influence on the structure, so the original melting time (2 h) was reduced to one hour.

Table 2 shows the general temperature programme for all the samples except for the samples with different melting times.

Table 2 Temperature programme for the sample preparation

Temperature range [°C]	Time [h:min]
40 – 800	00:30
800 – 800	00:40
800 – 1200	00:20
1200 – 1200	01:00*

*except the samples with different melting times

For the final investigation of the structure of the oxide glasses, samples with different compositions were prepared to be able to investigate the influence of sodium oxide and alumina oxide in the ternary borate glass system. *Figure 16* shows the composition diagram for the Na_2O-B_2O_3-Al_2O_3 system. The numbers refer to the fraction of each oxide in mol%. All samples prepared in this thesis are marked with a circle at its corresponding composition. The green empty circles mark the sample composition of the glasses doped with 0.1 mol% europium oxide. The filled circles mark the composition of the samples, which were, on the one hand, prepared with 0.1 mol% europium oxide and, on the other hand, with 0.1 mol% neodymium oxide.

The sample compositions were based on the work of Gresch and Müller-Warmuth [12], who did NMR studies of NABAL glasses.
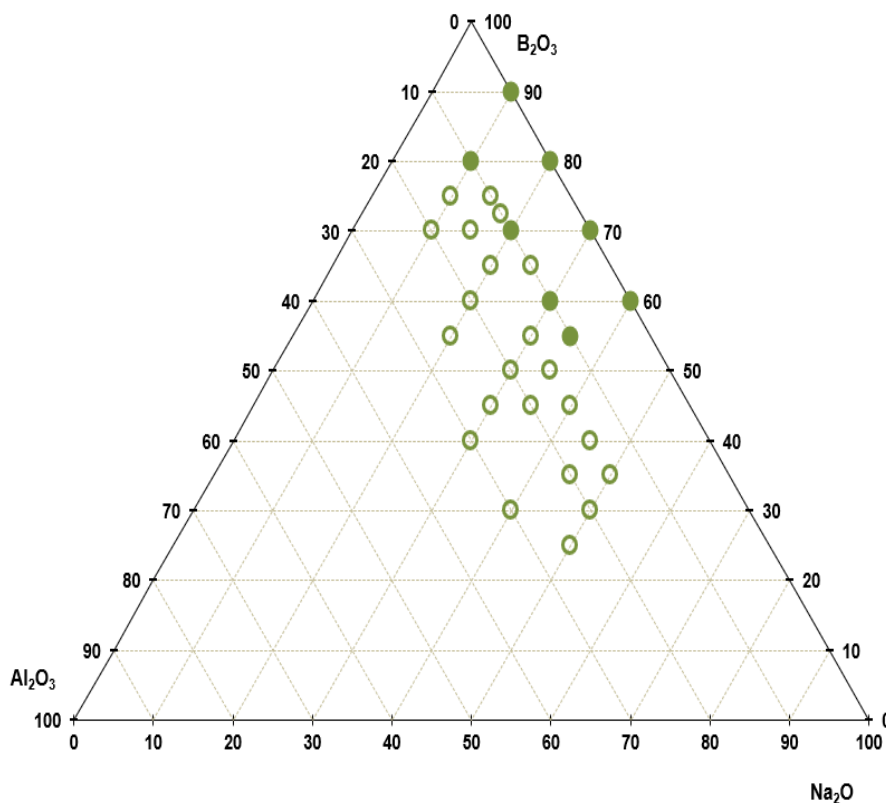
Figure 16 Composition diagram for the NABAL system with the samples investigated. The circles indicate the compositions of the prepared samples. The non-filled circles correspond to samples doped with 0.1 mol% Eu_2O_3 and the filled circles correspond to samples doped with 0.1 mol% Nd_2O_3.

A short-cut notation for the sample compositions is used as follows:

sodium oxide concentration in mol% - boron trioxide concentration in mol% - aluminium oxide concentration in mol%

For example, the sample name "10-80-10" corresponds to the sample with the composition 10 mol% Na_2O, 80 mol% B_2O_3 and 10 mol% Al_2O_3. The doping compound is always mentioned separately.

2. X-ray diffraction analysis

XRD analysis was necessary for the investigation of some samples, which were not transparent but had a milky colourless appearance, although according to the work of Gresch and Müller-Warmuth, they were supposed to be glassy. For other samples, a significant residual remained in the platinum crucible containing colourless powder or crystals. In order to get information about these phenomena, XRD measurements were performed. For the performance of these measurements it was necessary to crush and mill pieces of the samples in a mortar.

The following samples (all doped with 0.1 mol% Eu_2O_3) respectively crucible residuals were analysed by XRD analysis:

- 10-75-15 crucible residual (sample name XRD: GAT_ED1)
- 15-75-15 crucible residual (sample name XRD: GAT_ED2)
- 40-45-15 (sample name XRD: GAT_ED3)
- 45-40-15 (sample name XRD: GAT_ED4)
- 50-35-15 milky (sample name XRD: GAT_ED5)
- 50-35-15 transparent (sample name XRD: GAT_ED6)

Concerning the samples 50-35-15 milky and 50-35-15 transparent, one must mention that the transparent part was one drop of the melt quenched on a copper plate without the surrounding of a moult.

Figure 17 shows the row data XRD spectra of all the measured samples.
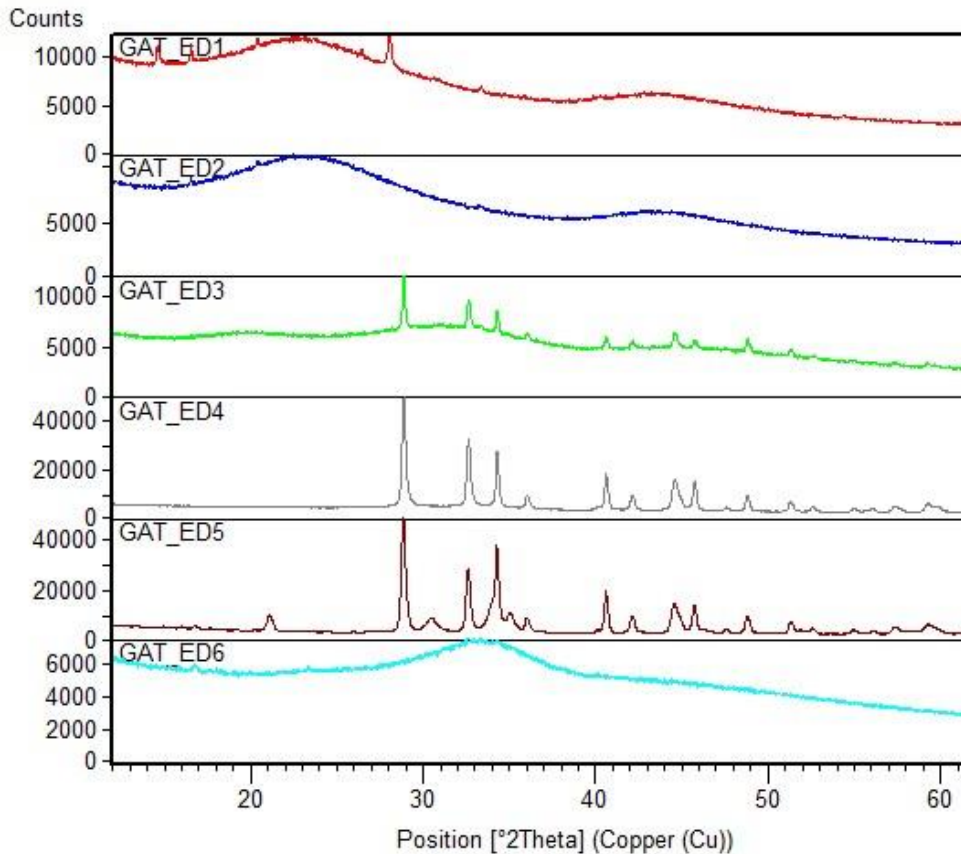
Figure 17 Overview row data XRD spectra of the samples 10-75-15 crucible residuals (GAT_ED1), 15-75-15 crucible residual (GAT_ED2), 40-45-15 (GAT_ED3), 45-40-15 (GAT_ED4), 50-35-15 milky (GAT_ED5), 50-35-15 transparent (GAT_ED6)

The XRD analysis shows that the crucible residuals of the samples 10-75-15 (GAT_ED1) and 15-75-15 (GAT_ED2) and the transparent sample part of sample 50-35-15 (GAT_ED3) are basically amorphous with a very small crystalline fraction, which is too small to be identified via XRD analysis.

In the samples 40-45-15 (GAT_ED3), 45-40-15 (GAT_ED4) and 50-35-15 milky (GAT_ED5) $Na(BO_2)$ (i.e. sodium metaborate) could be identified, whereas 45-40-15 (GAT_ED4) is the most pure one. Sample 50-35-15 (GAT_ED6) only shows amorphous features. From the comparison of sample 50-35-15 milky (GAT_ED5) and 50-35-15 transparent (GAT_ED6) one can see, that the quenching method and the subsequent heat treatment has an influence on the glass formation process. Thus, for the investigations carried out in this thesis it is important that the quenching method is always the same in order to receive comparable results.

Figure 18 to *Figure 20* show the XRD data and results after Rietveld refining of the samples 40-45-15 (GAT_ED3), 45-40-15 (GAT_ED4) and 50-35-15 milky (GAT_ED5) with the result of the composition. The other spectra are not shown as the samples are basically amorphous and hence the identification of the compounds was not possible.
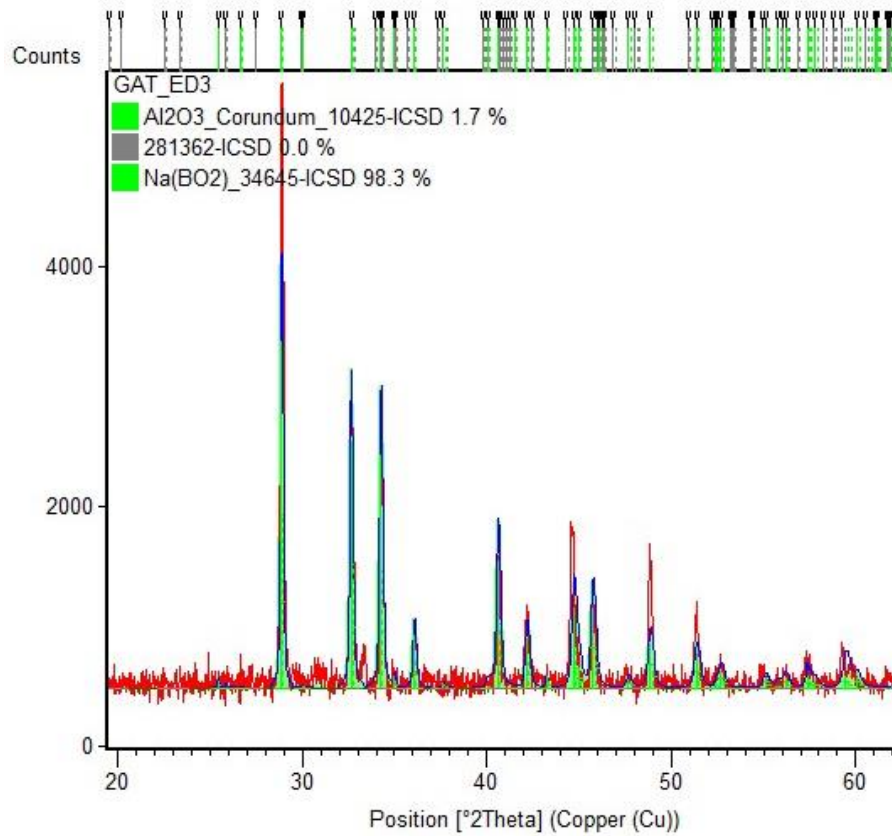
Figure 18 XRD spectrum of the sample 40-45-15 (GAT_ED3)

Figure 18 shows that the sample 40-45-15 (Eu_2O_3 doped) (sample name XRD: GAT_ED3) consists of 98.3% $Na(BO_2)$ and 1.7 % Al_2O_3.
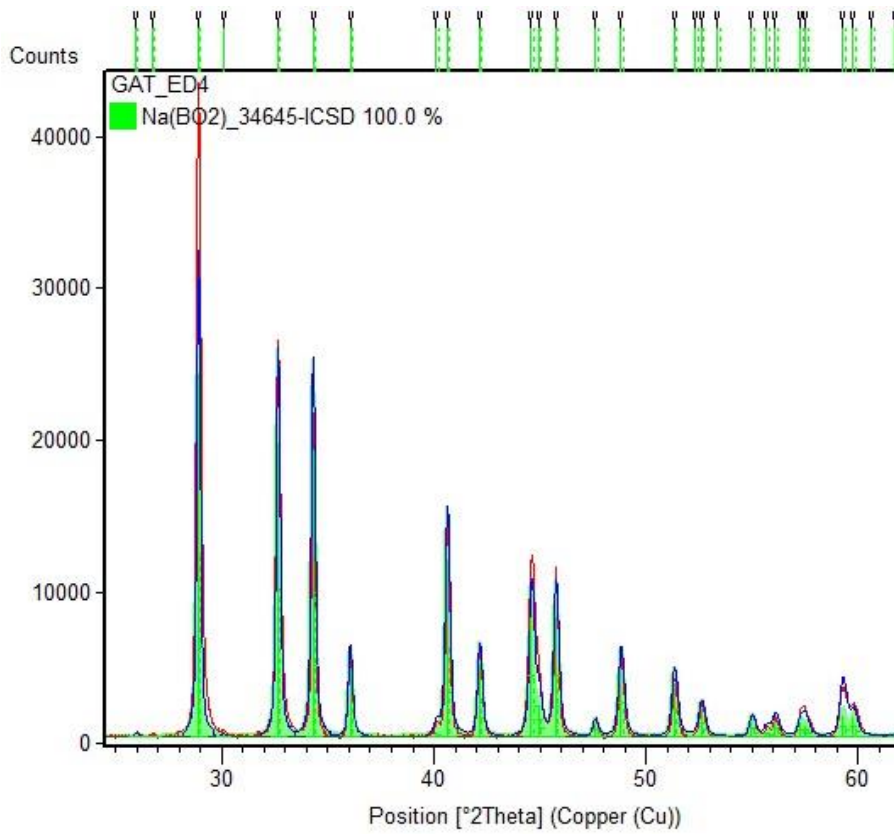
Figure 19 XRD spectrum of the sample 45-40-15 (GAT_ED4)
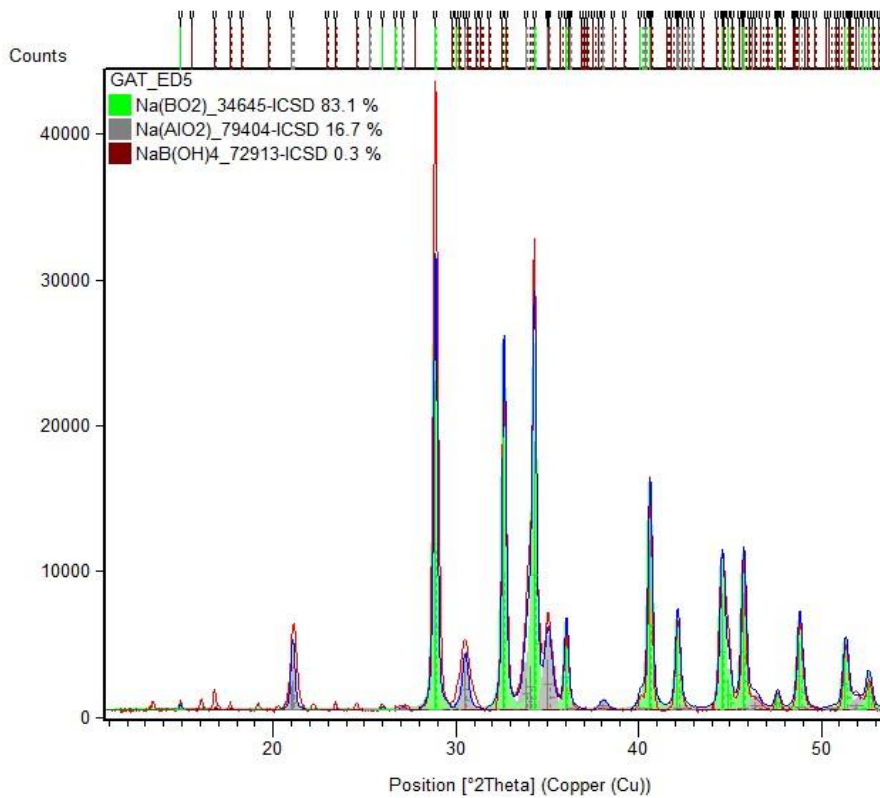
Figure 20 XRD spectrum of the sample 50-35-15 milky (GAT_ED5)

For the non-residual samples, represented in *Figure 18* and *Figure 19* the crystalline structures mainly containing $Na(BO_2)$ units can be clearly identified. Other components identified in the samples are Al_2O_3, $Na(AlO_2)$ and very small fractions of $NaB(OH)_4$ units. The sample 45-40-15 (Eu_2O_3 doped) is the most pure one with 100.0 % $Na(BO_2)$. Therefore, one can conclude that in the case of the sample 40-45-15 not all Al_2O_3 was included into the random network.

Due to the results of the XRD analysis, one can assume that the glass formation process is not the favoured process for the mentioned composition under the examined conditions. This shows that the amount of B_2O_3 as network former and Na_2O as network modifier plays an important role in the glass formation process.

Figure 21 shows the composition diagram for the investigated system with the modified glass formation region and with the circles indicating the prepared samples.
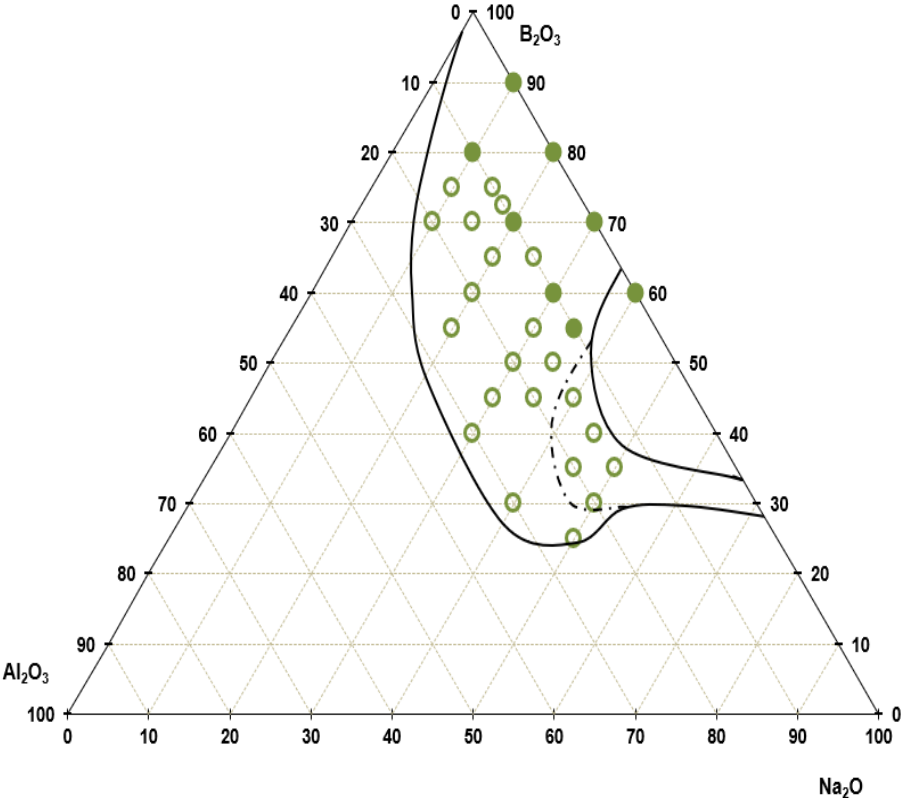
Figure 21 Composition diagram for the NABAL system with the samples investigated. The circles indicate the compositions of the prepared samples. The non-filled circles correspond to samples doped with 0.1 mol% Eu_2O_3 and the filled circles correspond to samples doped with 0.1 mol% Nd_2O_3. The solid line encloses the glass formation region proposed by Gresch and Müller-Warmuth. The dashed line shows the glass formation region modified in the frame of this thesis.

3. Determination of density by the Archimedian principle

The density of the samples was determined by the hydrostatic electronic balance *Mettler Toledo XS204 Delta Range*, which operates based on the Archimedian principle for the determination of density.

The Archimedian principle says that the upward buoyancy that a body is exposed to in a liquid equals the weight of the liquid that the body replaces. Thus, the hydrostatic balance calculates the density of the samples by its weight difference in air and in water. [74]

4. Spectroscopy

The samples were investigated by recording luminescence and/or transmission spectra.

4.1. Luminescence spectroscopy

4.1.1. Spectrometer

For the recording of all luminescence spectra (only samples doped with Eu_2O_3), a *Perkin Elmer LS55 fluorescence spectrometer* was used.

The LS55 spectrometer uses a pulsed xenon discharge lamp as light source, emission monochromator and filter, excitation monochromator and filter and a detector system, which consists of two photomultipliers covering a range from 200 to 900 nm.

The instrumental settings involving the operating mode, emission/excitation wavelength, emission and excitation slit, and detector gain can be varied. The device has the possibility to operate in the fluorescence, phosphorescence and chemiluminescence modes. For this thesis the fluorescence and the phosphorescence mode are of interest. These two modes differ in the internal sequence of the recording of the data. The fluorescence mode records the short-lived luminescence of the sample. This means that the detection of the emission signal commences at the peak of the excitation pulse. The emission of the light source and dark current are subtracted from the signal, which is measured when the excitation pulse is over. The phosphorescence mode records the luminescence with a determined delay after the excitation pulse for a determined time (gate). [75]

4.1.2. Procedure

The sample was placed in the sample chamber. At the beginning of the measurements, a luminescence spectrum with one of the predefined methods was recorded to get an overview on the sample's optical characteristics focusing on its luminescence maxima. Further, excitation spectra were recorded to identify the optimum excitation wavelength for the

luminescence spectra. These first steps were carried out at the beginning of each series, to get the best comparable parameters for each series. *Figure 22* shows the excitation spectrum of an arbitrarily chosen sample.
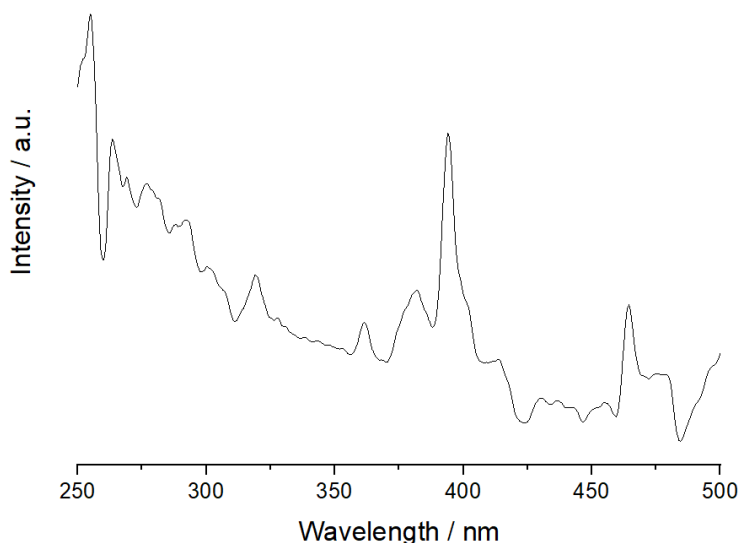
Figure 22 Excitation spectrum of Eu^{3+} in glass matrix

For the recording of the luminescence spectrum, the excitation wavelength is fixed, while the detection wavelength of the spectrometer is scanned. For the excitation spectrum, the emission wavelength is fixed, while the excitation wavelength is scanned.

In general, there could not be observed any afterglow after the excitation with the UV lamp. Therefore, it was presumed that the fluorescence mode was appropriate for the measurements. As the recorded emission showed very low intensities, the phosphorescence mode with a delay of 0.0 ms was used leading to higher intensities. This is in accordance with other solid samples presented in literature. It is assumed that a slight afterglow, invisible for human's eye, causes an incorrect dark current signal and consequently a wrong spectrum is recorded. [76]

Hence, for the monitoring of the emission spectra, the phosphorescence mode was used with the delay time set to 0.0 ms for every cycle.

4.1.3. Measurements

The parameters for the measurements were set for each series. *Table 3* to *Table 6* show the parameters for each series.

Series: Reduction of Eu^{3+} to Eu^{2+}: Influence of the melting time		
Fixed parameters	method	phosphorescence
	delay [ms]	0.00
	gate [ms]	1
	λ_{exc} [nm]	319
	$slit_{em}$ [nm]	5
	$slit_{exc}$ [nm]	5
	detector gain [V]	900
Samples	15-75-15 doped with Eu_2O_3 with different melting times: 1 h – 1 h 15 min – 1 h 30 min – 1 h 45 min – 2 h	

Series: Symmetry of the surrounding: Influence of the melting time		
Fixed parameters	method	phosphorescence
	delay [ms]	0.00
	gate [ms]	1
	λ_{exc} [nm]	394
	$slit_{em}$ [nm]	5
	$slit_{exc}$ [nm]	5
	detector gain [V]	775
Samples	15-75-15 doped with Eu_2O_3 with different melting times: 1 h – 1 h 15 min – 1 h 30 min – 1 h 45 min – 2 h	

Series: Symmetry of the surrounding: Influence of the alkali oxide content		
Fixed parameters	method	phosphorescence
	delay [ms]	0.00
	gate [ms]	1
	λ_{exc} [nm]	394
	$slit_{em}$ [nm]	varying (5 to 8)
	$slit_{exc}$ [nm]	varying (5 to 8)
	detector gain [V]	775 or 900
Samples	all samples doped with Eu_2O_3 at constant aluminium oxide content	

Series: Symmetry of the surrounding: Influence of aluminium oxide content		
Fixed parameters	method	phosphorescence
	delay [ms]	0.00
	gate [ms]	1
	Λ_{exc} [nm]	394
	$slit_{em}$ [nm]	varying (5 to 8)
	$slit_{exc}$ [nm]	varying (5 to 8)
	detector gain [V]	775 or 900
Samples	all samples doped with Eu_2O_3 at constant sodium oxide content	

4.2. Absorption spectroscopy

4.2.1. Spectrometer

For the recording of the absorption spectra, the *Perkin Elmer UV/VIS/NIR spectrometer Lambda950* was used because of its better spectral solution compared to the LS55.

The system consists of two different light sources, a deuterium lamp for the UV region (200 – 380 nm) and a tungsten halogen lamp for the VIS (380 – 780 nm) and the NIR region (780 – 2500 nm). As detectors, a photomultiplier tube (PMT) for the UV/VIS range and an InGaAs (or PbS) detector for the NIR are utilized. At 810 nm the change of the detector is executed automatically by the device. Sometimes this can be seen in the plotted spectrum. An integrating sphere (*150nm InGaAs Int. Sphere*) is mainly used for the reflection mode and an *UV/VIS/NIR accessory 2D detector module* is used for transmission/absorbance recordings. [77]

4.2.2. Procedure

Before the actual measurement of the sample, for samples doped with Nd_2O_3 a baseline was recorded with the settings necessary for the actual record. Therefore, as a reference an empty specimen holder (reference: air) was used. For samples doped with Eu_2O_3, no baseline correction was made. Further, these samples were placed in the closer to the detector (directly in front of the integrating sphere) to obtain higher intensities for weak bands. For both types of samples, a certified reflectance standard by *labsphere* was used for the integrating sphere.

4.2.3. Measurement

The parameters for the measurements were not varied within the series of Eu_2O_3 doped samples and not within the series of Nd_2O_3 doped samples. *Table 7* gives an overview on the parameters used for the series. All the other parameters were applied as originally set in the software, i.e. the default values.

Table 7 Parameters for the absorption measurements

Samples	Range [nm]	Data interval [nm]	Slit (PMT) [nm]
Eu_2O_3: 15-75-10	340-800/ 570-600	1/ 0.01	2
Nd_2O_3: all samples	400-700	0.01	2

V Results and discussion

This chapter involves the results and the discussion of them. In the first part of this section, pictures of all the samples are shown. In the following, the reduction of Eu^{3+} to Eu^{2+} is investigated in dependence of the melting time. Further parts focus on europium and neodymium as structural probes in glasses. As mentioned in the theoretical part, for the structural investigations of glasses via RE spectroscopy some element/ion specific transitions are important to focus on. Therefore, the hypersensitive transition of Eu^{3+} and both the hypersensitive transition and the nephelauxetic effect of neodymium ions were investigated. Moreover, calculations of the densities, optical basicities, molar volumes, packing ratios and substructure amounts are included.

1. Overview on the prepared samples

Table 8 and *Table 9* give an overview on the samples prepared in the frame of this thesis.

Table 8 Glass samples of the prepared europium doped samples photographed in daylight and under UV light (254 nm and 365 nm)

1.1. SAMPLES DOPED WITH 0.1 mol% Eu_2O_3	
Different melting times with constant composition (15-75-10): **1 h – 1 h 15 min – 1 h 30 min – 1 h 45 min – 2 h**	
daylight	
254 nm	
365 nm	
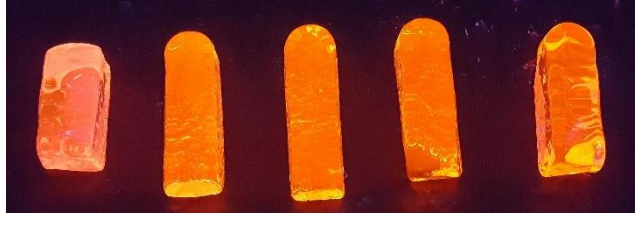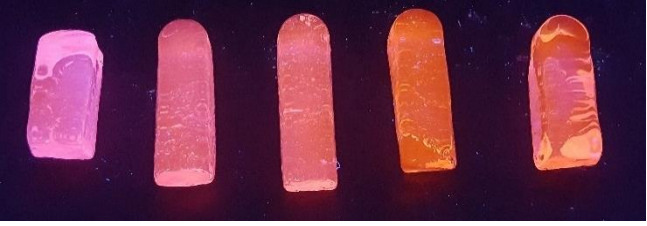
0 mol% Al₂O₃: 10-90-0, 20-80-0, 30-70-0, 40-60-0	
daylight	
254 nm	
365 nm	
10 mol% Al₂O₃: 15-75-10, 17.5-72.5-10, 20-70-10, 25-65-10, 30-60-10, 35-55-10	
daylight	
254 nm	
365 nm	
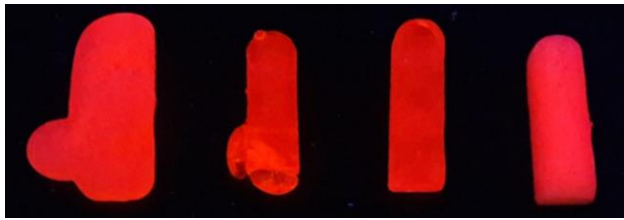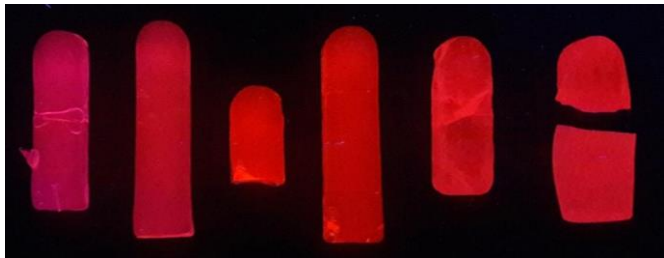
	15 mol% Al$_2$O$_3$:
	10-75-15, 15-70-15, 20-65-15, 30-55-15, 35-50-15, 40-45-15, 45-40-15, 50-35-15
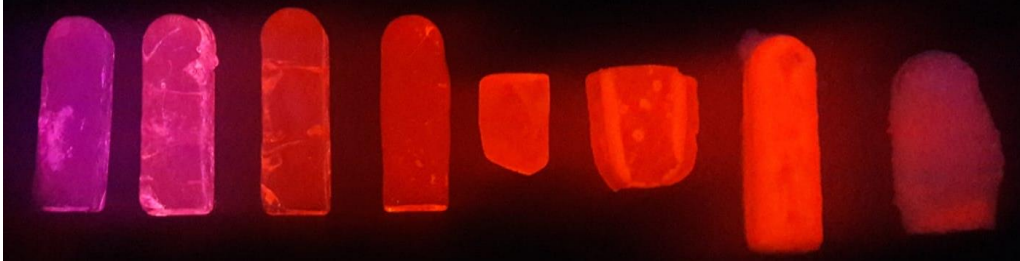
daylight	
254 nm	
365 nm	
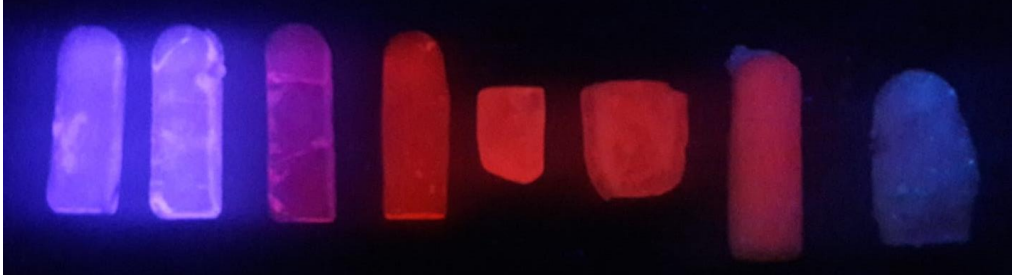
	20 mol% Al$_2$O$_3$: 10-70-20, 20-60-20, 30-50-20, 35-45-20, 50-30-20
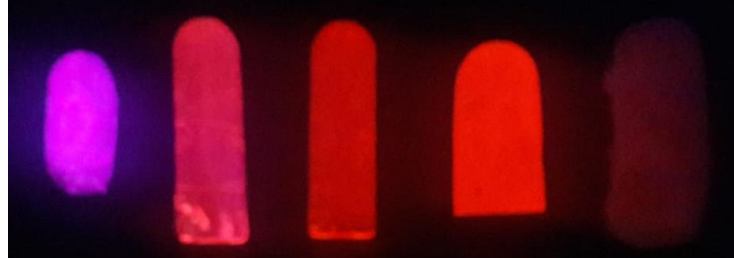
daylight	
254 nm	
365 nm	
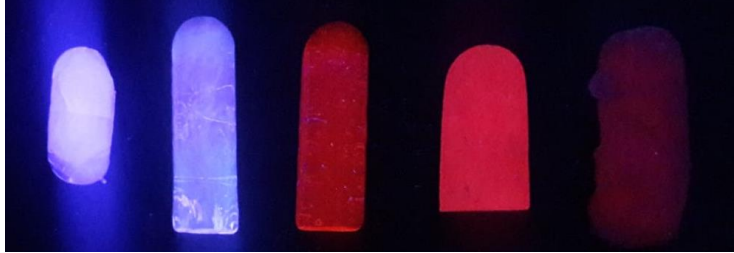
25 mol% Al₂O₃: 20-55-25, 30-45-25, 50-25-25	
daylight	
254 nm	
365 nm	
30 mol% Al₂O₃: 30-40-30, 40-30-30	
daylight	
254 nm	
365 nm	
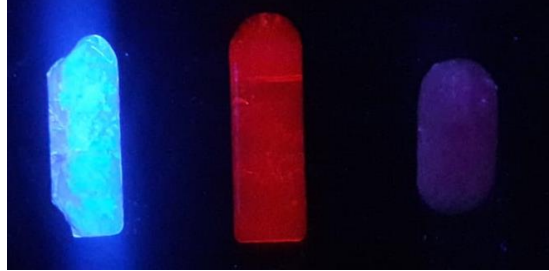
1.2. SAMPLES DOPED WITH 0.1 mol% Nd_2O_3	
0 mol% Al_2O_3: 10-90-0, 20-80-0, 30-70-0, 40-60-0	
daylight	
10 mol% Al_2O_3: 10-80-10, 15-75-10, 17.5-72.5-10, 20-70-10, 25-65-10, 30-60-10, 35-55-10	
daylight	

2. Optical investigations

2.1. Reduction of Eu^{3+} to Eu^{2+}: Influence of the melting time

In this section, the influence of the melting time on the reduction of Eu^{3+} to Eu^{2+} is investigated. Therefore, five samples featuring a composition of 15-75-10 and 0.1 mol% Eu_2O_3 were prepared. The samples were subject to different times of heat treatment (1 h, 1 h 15 min, 1 h 30 min, 1 h 45 min, 2 h).

Figure 23 shows the emission spectra of the prepared samples, recorded at an excitation wavelength of 319 nm, baseline corrected and normalized for the Eu^{3+} maximum at about 613 nm.
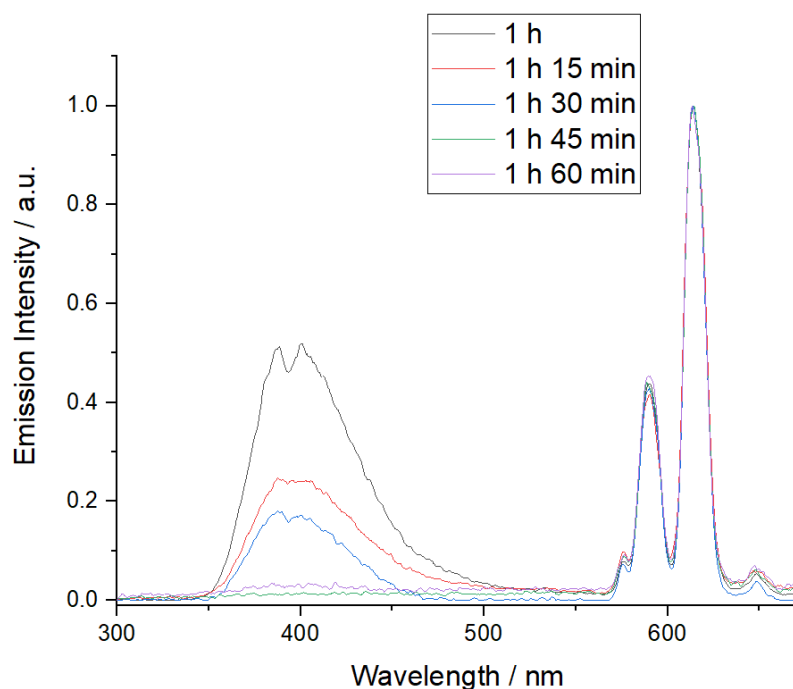
Figure 23 Emission spectra of the samples prepared with different melting times obtained after excitation of 319 nm

Figure 23 shows a decrease of the Eu^{2+} feature (broad emission band around 400 nm) in dependence of the melting time. The spectra clearly show that with the melting time in the oxidizing atmosphere of the oven the amount of the reduced species Eu^{2+} decreases. At melting times up to 1 h 30 min, the reduced species can be detected. For melting times longer than 1 h 30 min, apparently the oxidized form Eu^{3+} becomes the dominant species, as the band of the reduced species does not appear any longer in the spectra.

Figure 24 illustrates the ratio of Eu^{2+}/Eu^{3+} content calculated from the corresponding band areas with the melting time. The black line is included to guide the eye.
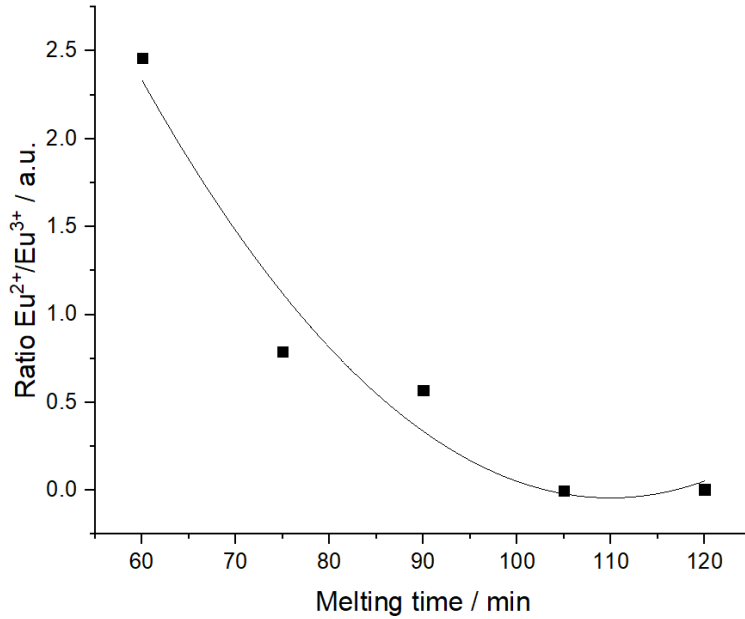
Figure 24 Ratio of Eu^{2+} to Eu^{3+} in the glass samples as a function of the melting time in min

Figure 24 shows that the reduction probability decreases with an increase of the melting time. This is in accordance with the results of Neuhold. [78]

2.2. Europium as structural probe in glasses: Symmetry of the surrounding

The hypersensitive transition $^5D_0 \rightarrow {}^7F_2$ of Eu^{3+} is used to investigate the site symmetry and the polarizability of the ligands. Both the site symmetry and the polarizability contribute to the covalency of the bonds.

To investigate these changes, the ratio of the $^5D_0 \rightarrow {}^7F_2$ (ED) and the $^5D_0 \rightarrow {}^7F_1$ (MD) is calculated. This ratio is also called asymmetry ratio (AS) described by *Formula* (5).

$$AS = \frac{A({}^5D_0 \rightarrow {}^7F_2)}{A({}^5D_0 \rightarrow {}^7F_1)} \tag{5}$$

A is the area of the bands of the corresponding transitions in parenthesis.

AS serves as a measure for the degree of distortion from inversion symmetry of the surrounding of the RE dopant ion. A larger ratio indicates a decreasing site symmetry and an increase of the polarizability of the ligands corresponding to an increase of covalency. For the calculation of AS, the recorded spectra were fitted, baseline corrected, normalized to the value 1 for the Eu^{3+} emission band, and integrated via *OriginLab software*.

45

To demonstrate the relevant changes, the extended region of the hypersensitive transition $^5D_0 \rightarrow {}^7F_2$ of an arbitrarily chosen spectrum, recorded at an excitation wavelength of 394 nm, baseline corrected and normalized for the Eu^{3+} maximum at about 613 nm, is shown in *Figure 25*.
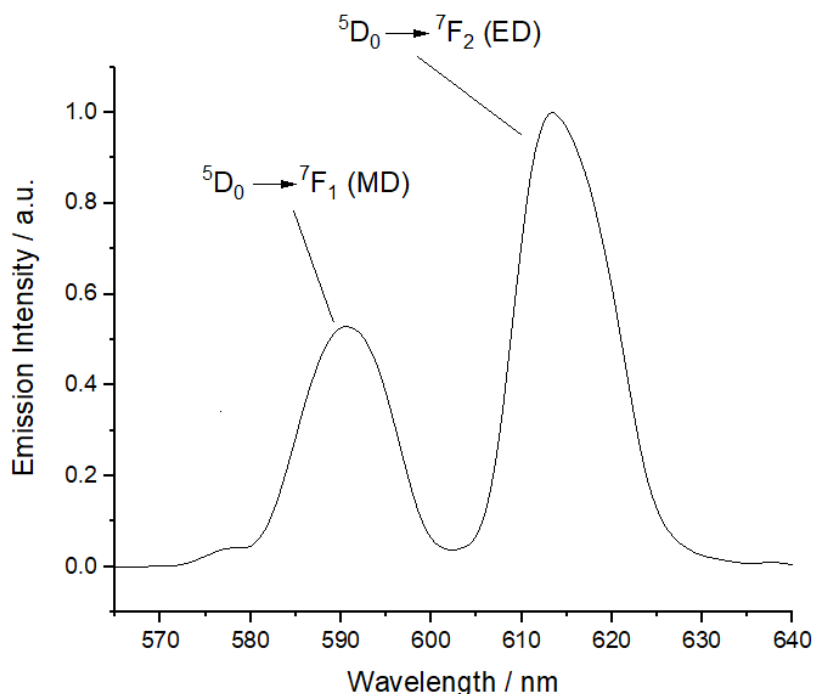

Figure 25 Emission spectrum of Eu³⁺ in glass matrix obtained after excitation at 394 nm showing ED and MD

The electric and magnetic dipole forbidden $^5D_0 \rightarrow {}^7F_0$ transition is located around 575 nm. This band could be observed in all monitored spectra. Its occurrence indicates that the RE ion occupies a site with C_{nv}, C_n or C_s symmetry.

$^5D_0 \rightarrow {}^7F_1$ (MD) is centred between 580 and 600 nm showing a poorly resolved Stark splitting. The most intense emission is observed at about 613 nm corresponding to $^5D_0 \rightarrow {}^7F_2$ (ED). The $^5D_0 \rightarrow {}^7F_2$ transition is magnetic-forbidden and electric-dipole allowed in odd field and strongly depends on the site symmetry (hypersensitive). MD does not depend strongly on the site.

In the following, it is demonstrated, how AS (ratio of ED to MD) and therefore, how the symmetry of the surrounding of the Eu^{3+} ion changes with the melting time, with the sodium oxide and with the aluminium oxide content.

2.2.1. Influence of the melting time

In this section, the influence of the melting time on the structure is investigated. Therefore, five samples featuring a composition of 15-75-10 and 0.1 mol% Eu_2O_3 were prepared. The samples were exposed to different times of heat treatment (1 h, 1 h 15 min, 1 h 30 min, 1 h 45 min, 2 h). *Figure 26* shows the emission spectra of the extended region of the hypersensitive transition of the samples with different melting times, recorded at an excitation wavelength of 394 nm, baseline corrected and normalized for the Eu^{3+} maximum at about 613 nm.
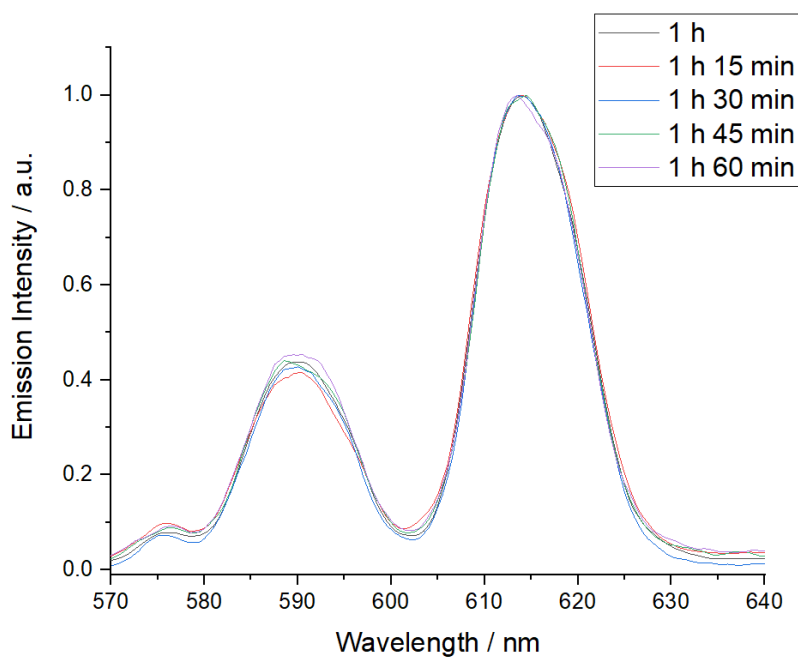
Figure 26 Emission spectra of the samples prepared with different melting times obtained after excitation at 394 nm

As it can be readily seen from the spectra in *Figure 26*, the intensities of ED and MD hardly change with an increase of the melting time.
Figure 27 shows AS as a function of the melting time.
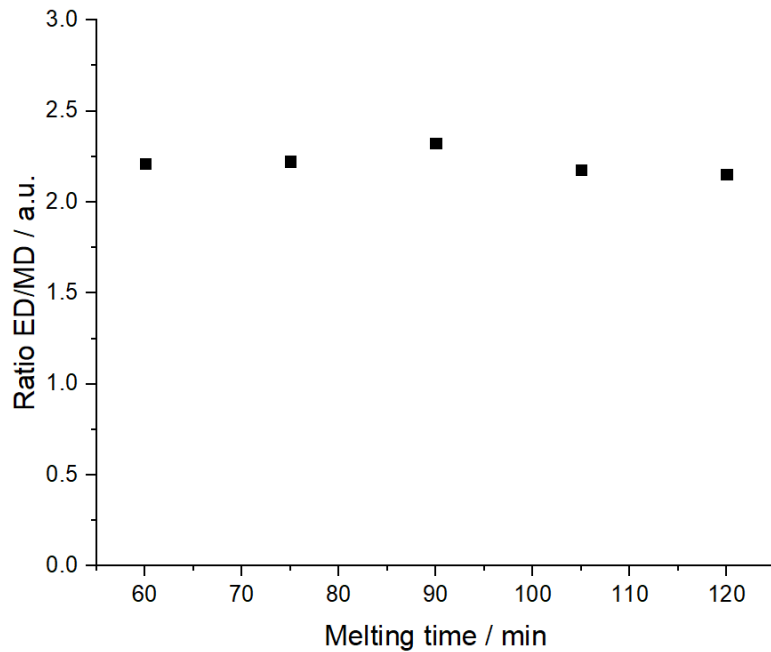
Figure 27 Ratio of ED/MD as a function of the melting time in min

Figure 27 proves that the melting time does not have any significant influence on the symmetry of the surrounding as the values of AS do not show any significant changes with an increase of the melting time.

2.2.2. Influence of the alkali oxide content

In this section, the influence of the sodium oxide content on the symmetry of the surrounding is investigated. For this, five series featuring constant alumina oxide contents (0, 10, 15, 20 and 30 mol% Al_2O_3) were prepared.

To demonstrate the changes with the composition of the glasses in the spectra, as an example the hypersensitive region of an arbitrarily chosen series (20 mol% Al_2O_3) is shown in *Figure 28*. The spectra were recorded at an excitation wavelength of 394 nm, baseline corrected and normalized for the Eu^{3+} maximum at about 613 nm.
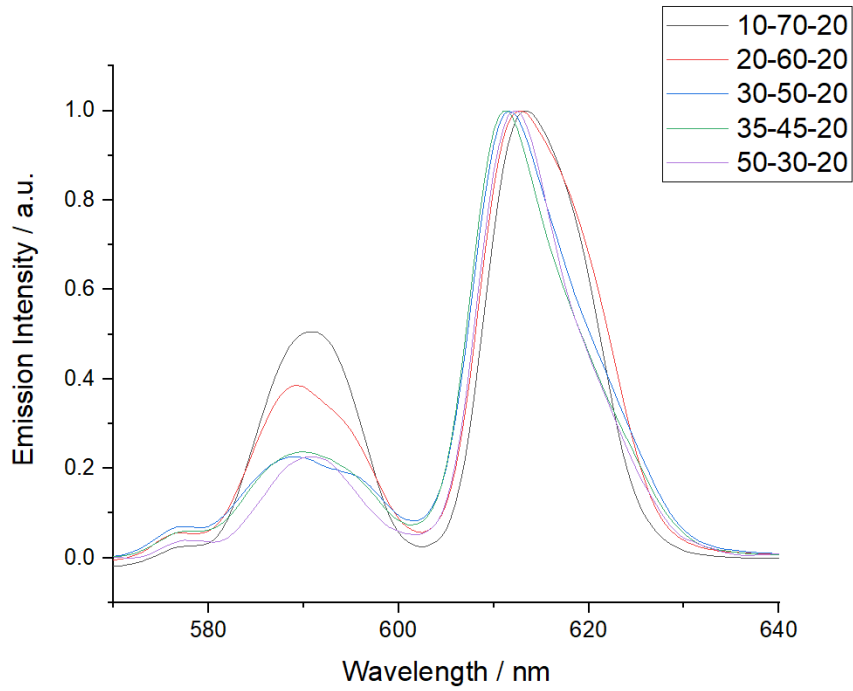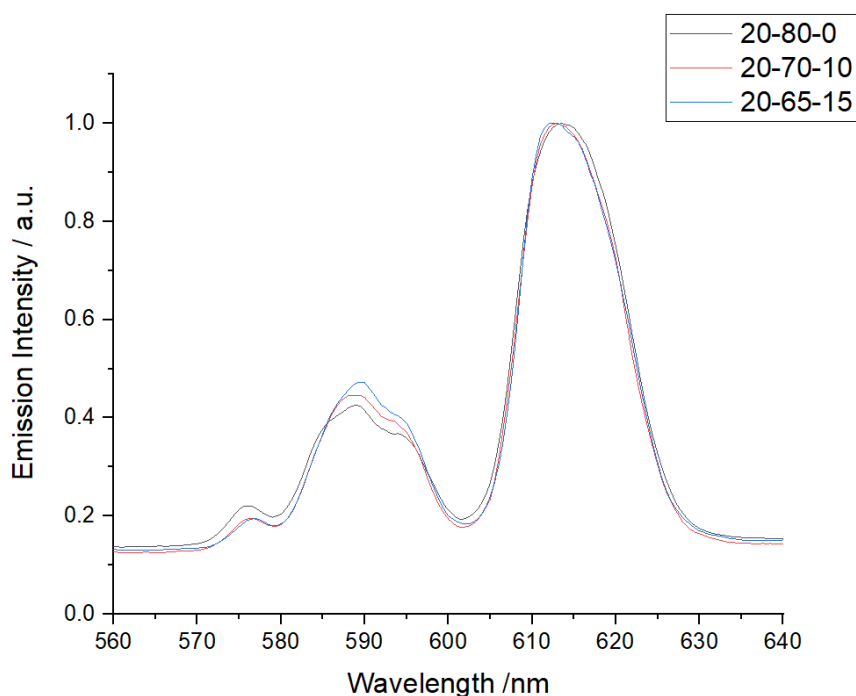
Figure 28 Emission spectra of the samples with different Na$_2$O concentration and constant Al$_2$O$_3$ concentration obtained after excitation wavelength of 394 nm

Figure 28 illustrates that the symmetry of the surrounding changes with different sodium oxide contents.

In *Figure 29* the values of AS for the series of the constant alumina oxide contents are plotted in dependence of the *R* (Na$_2$O/B$_2$O$_3$) values.
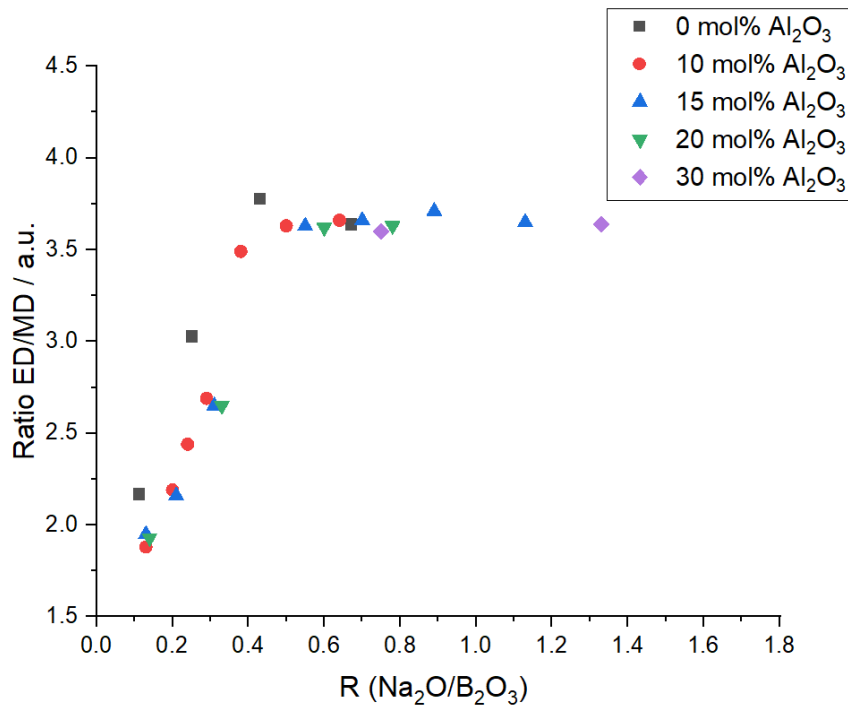
Figure 29 Ratio ED/MD as a function of R (Na$_2$O/B$_2$O$_3$)

Figure 29 shows an increase of AS up to *R* = 0.5. At higher *R* values it remains basically constant. Generally speaking, the symmetry of the surrounding of the RE ion undergoes changes until a value of *R* of about 0.5. Up to this value AS increases. Since a lower ED/MD value indicates a more symmetric surrounding, one can summarize that the site symmetry decreases the more sodium oxide (network modifier) the glass contains. With a further increasing sodium oxide content, no relevant changes in site symmetry can be observed.

This corresponds to an increasing polarizability of the ligands of the RE ions and hence, the covalent character of the bonds between the RE ions and the ligands also increases up to *R* = 0.5. When the covalent character of a bond increases, the ionic character decreases. This means, that the electron density between the ions forming the bond, increases.

2.2.3. Influence of the aluminium oxide content

In this section, the influence of the aluminium oxide content on the symmetry of the surrounding is investigated. For this, five series featuring constant aluminium oxide contents (10, 20, 30, 35, 40 mol% Al_2O_3) were prepared.

To demonstrate the changes with the composition of the glasses in the spectra, as an example the hypersensitive region of an arbitrarily chosen series (20 mol% Al_2O_3) is shown in *Figure 30.* The spectra were recorded at an excitation wavelength of 394 nm, baseline corrected and normalized for the Eu^{3+} maximum at about 613 nm.

Figure 30 Emission spectra of the samples with different Al_2O_3 and constant Na_2O concentrations obtained after excitation at 394 nm

Figure 30 illustrates that the symmetry of the surrounding changes only slightly with different alumina oxide contents.

In *Figure 31* the values of AS for the series of the constant sodium oxide contents are plotted in dependence of the K (Al_2O_3 concentration in mol% divided by the B_2O_3 concentration in mol%) values.
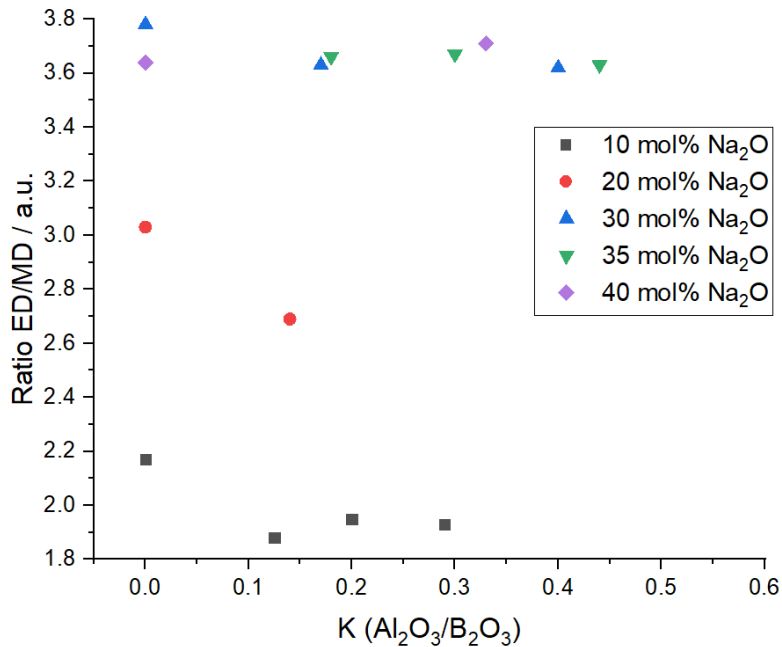
Figure 31 Ratio ED/MD as a function of K (Al_2O_3/B_2O_3)

Figure 31 shows that the ratio of ED/MD increases up to 30 mol% Na_2O. This could already be seen in *Figure 29* as 30 mol% correspond to an R value of 0.5. Further, it can be observed that for the samples without any Al_2O_3, the ratio is higher than for those, which contain Al_2O_3. Moreover, the alumina content has not so much influence on the ratio as the ratios stay constant within a range at constant sodium contents. In other words, with increasing Al_2O_3 contents the symmetry of the surrounding of the RE ion does not change significantly. This can be explained by the function of the oxides in the glass forming process. Na_2O is supposed to act as a network modifier whereas Al_2O_3 can act both as network former and as a network modifier. As the symmetry of the surrounding shows severe changes with increasing Na_2O content, it can be proven, that this oxide modifies the network up to an R value of 0.5. Hence, one can assume that Al_2O_3 tends to act more as network former than as network modifier, as its presence does not lead to any severe changes in symmetry.

51

2.3. Neodymium as structural probe in glasses

2.3.1. Symmetry of the surrounding

The hypersensitive transition $^4I_{9/2} \rightarrow {}^4G_{5/2}$ of Nd^{3+} is used to investigate the site symmetry and the polarizability of the ligands. Both the site symmetry and the polarizability correspond to the covalency of the bonds.

Similar environments of the first coordination sphere of the RE ions produce similar shapes of the hypersensitive transition. Determining factors for the band shape of the hypersensitive transitions in oxide glasses are the type (bridging or non-bridging), number and the geometry of the oxygen ions around the RE ions.

Figure 32 shows the spectral region of the $^4I_{9/2} \rightarrow {}^4G_{5/2}$, $^2G_{7/2}$ transitions of the absorption spectra of the neodymium doped glasses. All spectra were recorded at room temperature (RT).
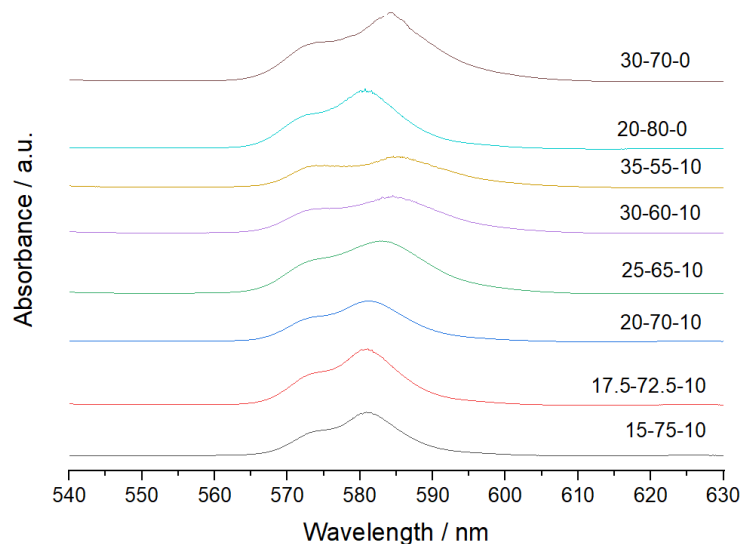
Figure 32 Absorption spectrum showing the extended hypersensitive region of the neodymium doped samples

The bands centred between about 570 and 595 nm is the most intense absorption band and refers to the $^4I_{9/2} \rightarrow {}^4G_{5/2}$, $^2G_{7/2}$ transition. The $^4I_{9/2} \rightarrow {}^4G_{5/2}$, the band at smaller energies, corresponds to the hypersensitive transition of the Nd^{3+} ion. Both bands are general badly resolved in glasses and in solutions. [78]

Nevertheless, one can draw some conclusions: As the shape of the bands in this region changes quite a lot as the modifier content is altered, one can assume that the environment of the RE ion changes very much with increasing modifier content. The samples with low modifier content show very similar band shapes. As oxide glasses, the environment refers to the number and geometry of oxygens. In the samples 30-70-0, 17.5-72.5-10 and 15-75-10 the hypersensitive transition is especially intense, which corresponds to more distortion from the inversion symmetry. Anyway, Reisfeld and Eckstein [79] suggested for thulium and erbium in

sodium silicate and sodium borate glasses C_2 as the predominant site symmetry with the overall coordination number eight which is made up by NBOs, which belong to the corners of the BO_4 tetrahedra. Each of these tetrahedra donates two oxygens. Generally speaking, eight is the most common coordination number in RE oxides.

2.3.2. Nephelauxetic effect

The transition $^4I_{9/2} \rightarrow {}^2P_{1/2}$ correlates with the nephelauxetic effect of the Kramer's ion Nd^{3+}.

At RT mainly transitions from the crystal-field split ground state multiplets $^4I_{9/2}$ to the unsplit $^2P_{1/2}$ state contribute to the intensity of this band. As already mentioned above, this system can be considered as a hot band system. Other contributions in terms of the intensity of this band have its roots in the close-lying $^2D_{5/2}$ state. Nevertheless, the overlap with this band is even at RT quite small. At low temperatures the band becomes sharper as only the lowest crystal field state of the ground state multiplets is populated. In this case, the transitions only take place between discrete and unsplit levels. This leads to the fact that now the FWHM of this band is determined by the variety of different sites that are occupied by the Nd^{3+} ions in the glass. Hence, at low temperatures the FWHM is a sensitive indicator for the internal structural changes.

The Racah parameter and spin-orbit coupling parameters mainly determine the positions of the $^{2S+1}L_J$ multiplets of Nd^{3+}. Changes of the positions have its origin in the nephelauxetic effect, which is, as already mentioned a measure for the covalency of the metal-oxygen bond. It occurs as a result from the expansion of the partly filled f-shell, which itself arises due to charge transfer from the ligands to the metal. The overlap results in a contraction of the energy level structure of the ion in the glass, which manifests itself in a shift towards smaller energies.

At low temperatures no peak shifts due to crystal field splitting can occur. In the frame of this thesis, this transition was only monitored at RT.

Figure 33 shows the peak positions of the $^4I_{9/2} \rightarrow {}^2P_{1/2}$ transition with increasing Na_2O content.
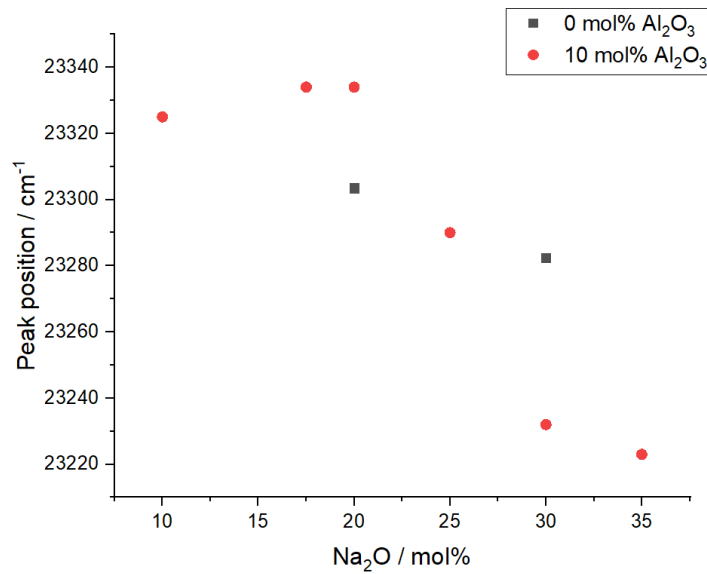
*Figure 33 Peak position of the of the transition $^4I_{9/2} \rightarrow {}^2P_{1/2}$
as a function of the Na_2O concentration in mol%*

The shift to smaller energies is greater with increasing Na_2O concentration. Hence, the bonds around the RE ion have a more covalent character. At very low Na_2O concentrations the covalent character is higher, then it slightly decreases around 20 mol% Na_2O and then it increases drastically. Beginning at 30 mol% the decrease already starts to be less drastic and therefore less changes in the surrounding are observed. Nevertheless, there must be mentioned that the spectra were monitored at room temperature, which results in the possibility of shifts of this band induced by crystal-field splitting effects.

Figure 34 shows the FWHM of the $^4I_{9/2} \rightarrow {}^2P_{1/2}$ transition as a function of the Na_2O concentration.
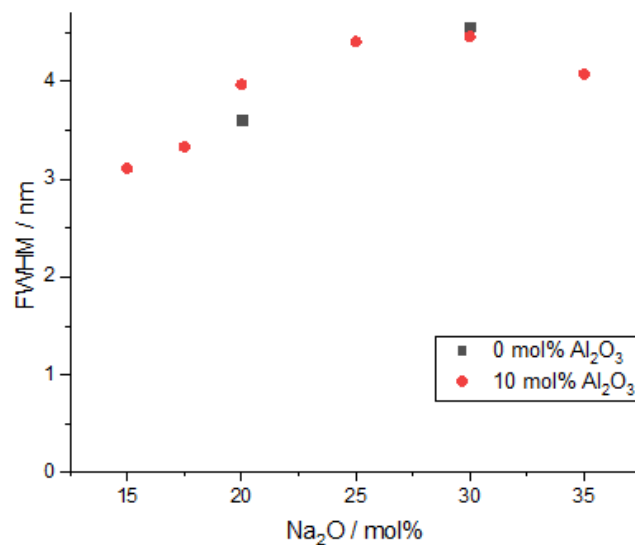
*Figure 34 FWHM of the transition $^4I_{9/2} \rightarrow {}^2P_{1/2}$ as a function
of the Na_2O concentration in mol%*

As already mentioned, the FWHM of the band of the $^4I_{9/2} \rightarrow {}^2P_{1/2}$ transition provides information on the diversity of the Nd^{3+} sites in the host material. Until 30 mol% the FWHM is increasing. It therefore represents the increasing disorder in the glass matrix. This increasing disorder can be explained by the change of the rather two-dimensional network to the rather three-dimensional network as the three-coordinated units are changed to four-coordinated units. Further, the formation of BO_4 units, which is forced by an increasing modifier content, enables closer packaging of the oxygens. This is, conversely, the reason for the increased overlapping of the partly filled f-shell with the ligands and therefore, for the nephelauxetic effect.

3. Densities

Figure 35 shows the determined densities of the prepared glass samples as a function of *K* (Al_2O_3/B_2O_3) and as a function of *R* (Na_2O/B_2O_3). For some samples, however, it was impossible to determine the density due to existing pores or due to hygroscopic behaviour.
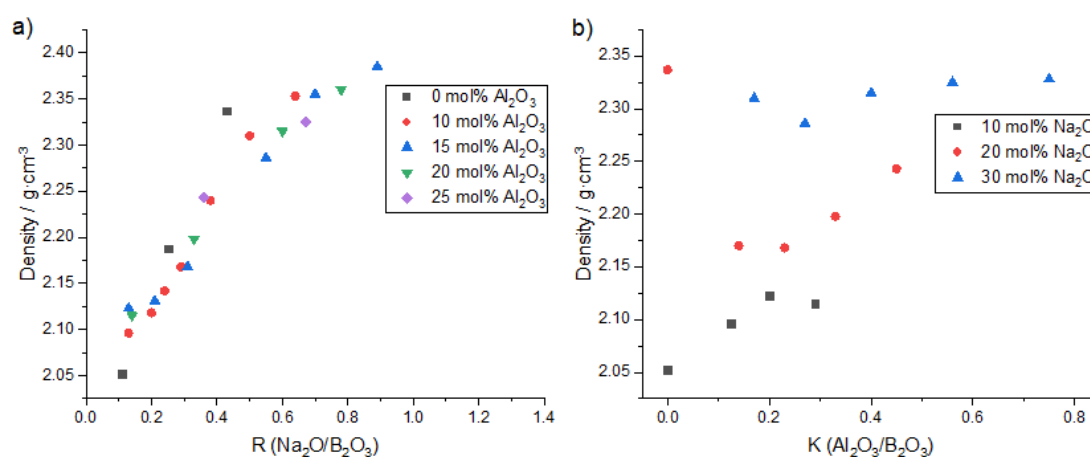
Figure 35 Densities of the prepared samples as a function of a) R (Na_2O/B_2O_3) and b) K (Al_2O_3/B_2O_3)

The density steadily increases with increasing the sodium oxide content. Also, it could be seen that the binary glasses, which do have an Al_2O_3 content of 0 mol% have higher densities than its ternary equivalents. With increasing aluminium oxide content, the density of the glasses with 20 and 30 mol% Na_2O show minima at $K = 0.23$ and 0.27. This corresponds to aluminium oxide contents of 15 mol%. Because of this, the obtained densities are in accordance with the densities reported by Doweidar *et al.* The situation is different for the samples of 10 mol% as they show a maximum of the density at $K = 0.2$.

4. Theoretical optical basicity

The concept of the theoretical optical basicity was introduced by Duffy and Ingram [80]. Based on the Lewis concept of acids and bases, it describes the electron donating ability of oxygen ions, which is also related to the polarizability of the oxygen ions. A larger oxygen polarizability correlates with a higher basicity and hence, a larger nephelauxetic effect, which also correlates with the concept of covalency of the Eu-O bond.

Nevertheless, is must be mentioned that the optical basicity contains average information, whereas the nephelauxetic effect is a measure of the local polarizability at the sites of the RE ions. Hence, the nephelauxetic effect and the optical basicity are not necessarily parallel. [81] The optical basicity is described by *Formula* (6). [80]

$$\Lambda_{th} = \chi_{AO_{\frac{a}{2}}} \Lambda\left(AO_{\frac{a}{2}}\right) + \chi_{BO_{\frac{b}{2}}} \Lambda\left(BO_{\frac{b}{2}}\right) + \dots \tag{6}$$

Λ_{th} theoretical optical basicity

$\Lambda\left(XO_{\frac{x}{2}}\right)$ optical basicity of oxides

$\chi_{XO_{\frac{x}{2}}}$ proportion of oxygen ions each cation contributes

The following calculation serves as an example for the calculation of the theoretical optical basicity. It is calculated for the sample 15-75-10. The values for the optical basicity of the oxides are fixed parameters and were taken from reference [80].

$$\Lambda_{th} = \frac{15}{270} * 1.15 + \frac{225}{270} * 0.42 + \frac{30}{270} * 0.60 = 0.481$$

Figure 36 represents the theoretical optical basicity as a function of the Na_2O concentration and as a function of the Al_2O_3 concentration in mol%.
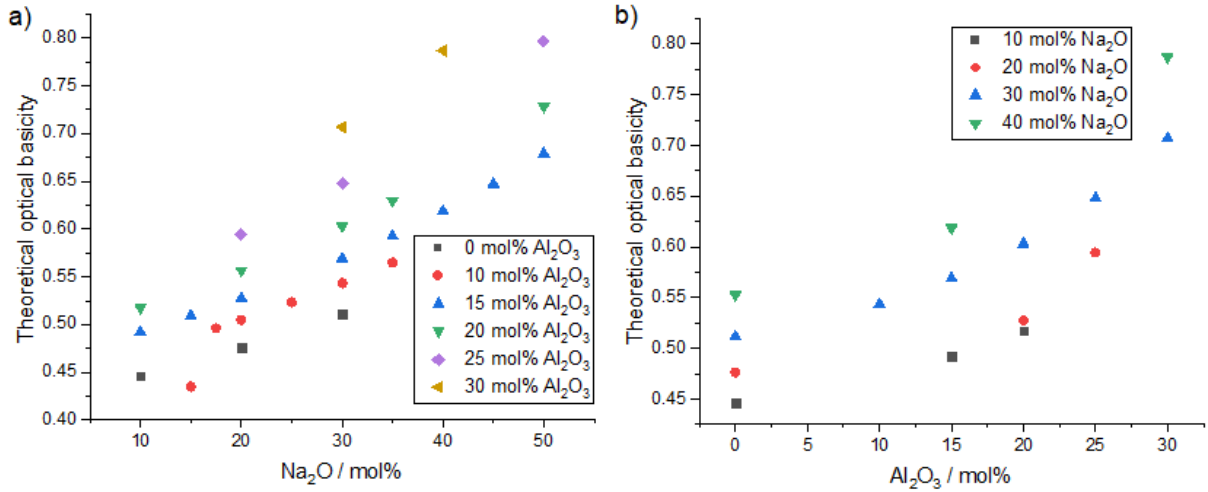
Figure 36 Theoretical optical basicity as a function of a) Na₂O content and b) Al₂O₃ content in mol%

Generally speaking, one must say that the larger the theoretical optical basicity, the larger is the polarizability of the oxygens in the surrounding of the RE ion. Nevertheless, it has to be highlighted that these values are calculated values and therefore, they do not necessarily correspond to the experimental data over the whole range. The optical basicity and therefore also the polarizability increase with increasing Na_2O and Al_2O_3 concentration according to the calculations of the optical basicity. Therefore, also the electron donating power increases.

5. Molar volumes and packing ratios

The molar volume, V_m, of the glasses can be calculated by *Formula* (4).

$$V_{\mathrm{m}} = \frac{M}{\rho} \tag{4}$$

M is the molecular weight in g·mol⁻¹ and ρ is the density in g·cm⁻³.

In literature [82] and [84] it is suggested that the ionic packing ratio, V_p, is a suitable measure for the relations between the properties and the structure of glasses. It can be calculated by *Formula* (7).

$$V_{\mathrm{p}} = \frac{\sum_i \frac{4}{3} \pi r_i^3 n_i N_A}{V_{\mathrm{m}}} \tag{7}$$

r_i ionic radius of species *i* according to Pauling in cm

n_i molar fraction of species *i*

N_A Avogadro constant in mol⁻¹

The following calculation serves as an example for the calculation of the packing ratios. It is calculated for the sample 15-75-10. The ionic radii according to Pauling were taken from the following sources:

$$V_{\mathrm{p}} = \frac{\frac{4}{3}\pi * 6.022 * 10^{23}\ mol^{-1}}{\frac{72.06\ g * mol^{-1}}{2.118\ g * cm^{-3}}} *$$

$$[(9.5 * 10^{-9}\ cm)^3 * 0.15 + (1.2 * 10^{-9}\ cm)^3 * 0.75 + (5.3 * 10^{-9} * 0.10)$$

$$+ \left(1.4 * 10^{-8} * (0.15 * 1 + 0.75 * 3 + 0.10 * 3)\right)]$$

$$= 0.5612$$

The radii were taken from the sources [85] for Na^+ and O^{2-} and [86] for B^{3+} and Al^{3+}.
Figure 37 shows the molar volume as a function of the Na_2O concentration and as a function of the Al_2O_3 concentration in mol%.
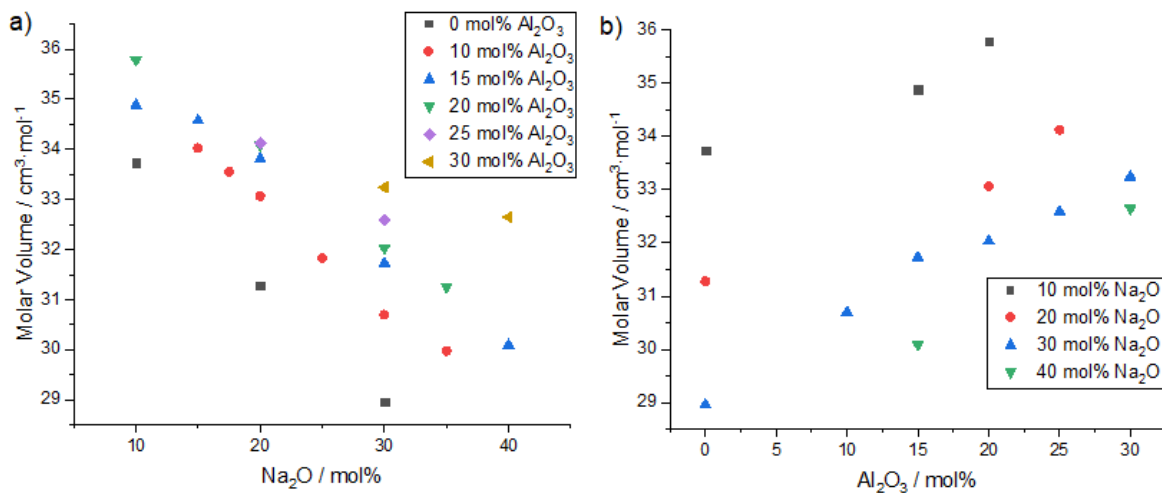
Figure 37 Molar volume as a function of a) Na₂O content and b) Al₂O₃ content in mol%

The molar volume decreases with increasing Na_2O content and increase with increasing Al_2O_3 content.
Figure 38 shows the packing ratio as a function of the Na_2O concentration and as a function of the Al_2O_3 concentration in mol%.
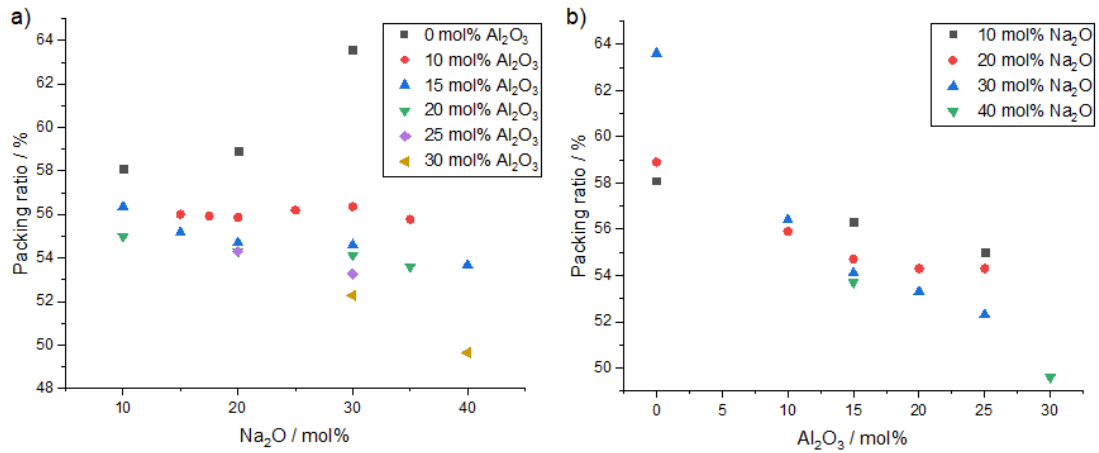
Figure 38 Packing ratio as a function of a) Na_2O content and b) Al_2O_3 content in mol%

Apart from the glasses with 0 mol% Al_2O_3 (increasing) and with 10 mol% Al_2O_3 (constant), the packing ratio decreases with increasing Na_2O contents. Further, with increasing Al_2O_3 contents, the packing ratio decreases.

6. Table representing Λ, AS, ρ, V_m, V_p

Table 10 Overview on R and K values, theoretical optical basicity, asymmetry ratio, density, molar volume and packing ratios of the prepared samples

Dopant	Sample		R (Na_2O/B_2O_3)	K (Al_2O_3/B_2O_3)	Theoretic optical basicity Λ	Asymmetry ratio AS	Density ρ [g·cm^{-3}]	Molar volume V_m [cm^3·mol^{-1}]	Packing ratio V_p [%]
0.1 mol% Eu$_2$O$_3$	melting times	1 h	0.20	0.13	0.49	2.21	2.122	33.96	56.1
		1 h 15 min				2.22	2.119	34.01	56.0
		1 h 30 min				2.32	2.123	33.94	56.1
		1 h 45 min				2.18	2.110	34.15	55.8
		2 h				2.15	2.099	34.33	55.5
	10-90-0		0.11	0	0.45	2.17	2.052	33.73	58.1
	20-80-0		0.25	0	0.48	3.03	2.188	31.28	58.9
	30-70-0		0.43	0	0.51	3.78	2.337	28.96	63.6
	40-60-0		0.67	0	0.55	3.64	-	-	-
	15-75-10		0.20	0.13	0.49	1.88	2.118	34.02	56.0
	17.5-72.5-10		0.24	0.14	0.50	2.19	2.142	33.55	55.9
	20-70-10		0.29	0.14	0.50	2.69	2.168	33.06	55.9
	25-65-10		0.38	0.15	0.52	3.49	2.240	31.83	56.2
	30-60-10		0.50	0.17	0.54	3.63	2.310	30.70	56.4
	35-55-10		0.64	0.18	0.56	3.66	2.353	29.98	55.8
	10-75-15		0.13	0.20	0.49	1.88	2.123	34.88	56.3
	15-70-15		0.21	0.21	0.51	2.16	2.131	34.57	55.2
	20-65-15		0.31	0.23	0.53	2.65	2.168	31.73	58.3
	30-55-15		0.55	0.27	0.57	3.63	2.286	31.73	54.6
	35-50-15		0.70	0.30	0.59	3.66	2.355	31.76	52.7
	40-45-15		0.89	0.33	0.62	3.71	2.385	30.09	53.7
	45-40-15		1.13	0.38	0.65	3.65	-	-	-
	50-35-15		1.43	0.43	0.68	o	-	-	-

- determination of the density was not possible, consequently V_m and V_p could not be calculated

o determination of AS was not possible

Dopant	Sample	R (Na$_2$O/B$_2$O$_3$)	K (Al$_2$O$_3$/B$_2$O$_3$)	Theoretic optical basicity Λ	Asymmetry ratio AS	Density ρ [g·cm^{-3}]	Molar volume V_m [cm^3·mol^{-1}]	Packing ratio V_p [%]
0.1 mol% Eu$_2$O$_3$	10-70-20	0.14	0.29	0.52	1.93	2.115	35.78	55.0
	20-60-20	0.33	0.33	0.56	2.65	2.198	34.0 8	54.3
	30-50-20	0.60	0.40	0.60	3.62	2.315	32.03	54.1
	35-45-20	0.78	0.44	0.63	3.36	2.360	31.26	53.6
	50-30-20	1.67	0.67	0.73	4.30	-	-	-
	20-55-25	0.36	0.45	0.59	o	2.243	34.12	54.3
	30-45-25	0.67	0.56	0.65	o	2.325	32.59	53.3
	50-25-25	2.00	1.00	0.80	o	-	-	-
	30-40-30	0.75	0.75	0.71	3.60	2.328	33.24	52.3
	40-30-30	1.33	1.00	0.79	3.64	2.347	32.65	49.6
0.1 mol% Nd$_2$O$_3$	10-90-0	0.11	0	0.45	•	2.047	33.80	58.0
	20-80-0	0.25	0	0.48	•	2.183	31.35	58.8
	30-70-0	0.43	0	0.51	•	2.334	28.99	59.6
	40-60-0	0.67	0	0.55	•	-	-	-
	15-75-10	0.20	0.13	0.49	•	2.123	33.94	56.1
	17.5-72.5-10	0.24	0.14	0.50	•	2.142	31.55	59.5
	20-70-10	0.29	0.14	0.50	•	2.170	33.02	55.9
	25-65-10	0.38	0.15	0.52	•	2.244	31.76	56.3
	30-60-10	0.50	0.17	0.54	•	2.319	30.57	56.6
	35-55-10	0.64	0.18	0.56	•	2.359	29.89	55.9

- determination of the density was not possible, consequently V_m and V_p could not be calculated

o determination of AS was not possible

• Nd$_2$O$_3$ → no determination of AS

7. Substructure amounts

As already described in the theoretical part the literature suggests some models on the structure of borate glasses. Anyway, for the calculation of the number of BO_4-units in NABAL glasses, *Formula* (8), proposed by Gresch and Müller-Warmuth [36],[37] is used.

$$N_4(B) = (1 - 0.031y)R \qquad (8)$$

R   ratio of the molfractions Na_2O and B_2O_3

y   concentration of Al_2O_3 in mol%

Figure 39 shows the $N_3(B)$ and $N_4(B)$ units as a function of *R* (Na_2O/Al_2O_3).
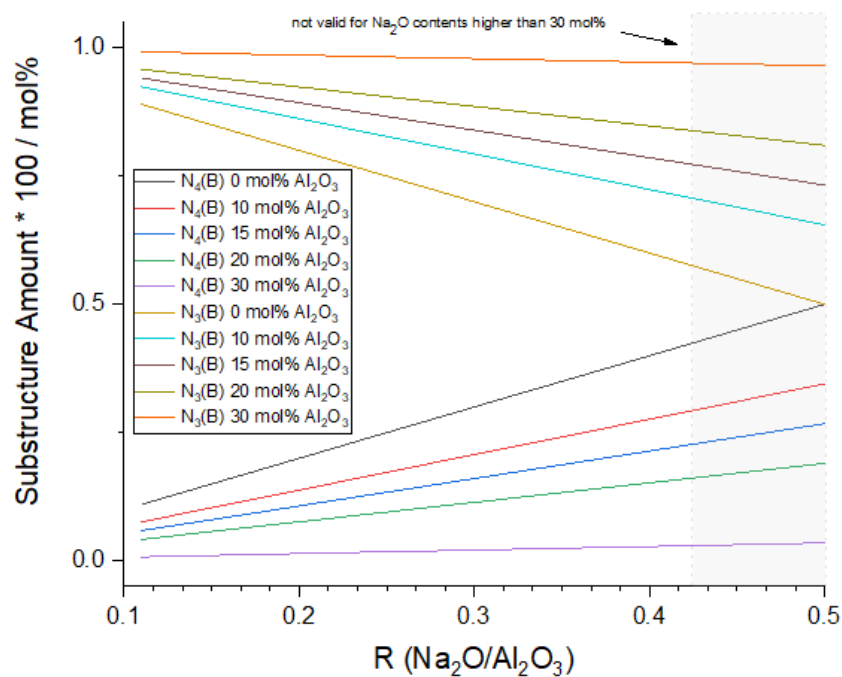
Figure 39 Substructure amount as a function of R (Na_2O/B_2O_3)

The slopes decrease with increasing Al_2O_3 contents for $N_4(B)$. This can be explained by the favoured formation of $N_4(Al)$ units in comparison to $N_4(B)$ units. As the amounts of the $N_3(B)$ units can be described as the boron atoms not converted to $N_4(B)$, its substructure amount is described by the rest of boron atoms. The calculations are only valid up to 30 mol% Na_2O.

VI Conclusion

The XRD measurements of the prepared glasses resulted in a modified glass formation region for NABAL glasses shown in *Figure 21*. Concerning the reduction of Eu^{3+} to Eu^{2+} it was concluded that the probability of the reduction decreases with an increase of the melting time. This is in accordance with the results of Neuhold.

The spectroscopic investigations of the europium samples prepared at different melting times showed that the melting time does not have any severe influence on the glass structure.

The compositional dependent changes in the optical spectra showed that up to 30 mol% Na_2O severe changes in the symmetry of the RE ions take place indicating more distortion from symmetry with increasing modifier content. This is in accordance with the results of Gresch and Müller-Warmuth, who proposed that the added modifier associates preferably with Al_2O_3, but also converts trigonally coordinated boron ($N_3(B)$) to four-coordinated boron ($N_4(B)$). This could be also proven by the FWHM of the nephelauxetic effect of the Nd^{3+} samples as it rises up to 30 mol% Na_2O and then starts decreasing. This rise indicates an increase in disorder of the environment, which corresponds to the transformation from the two-dimensional trigonally coordinated boron to the three-dimensional network referring to the four-coordinated boron.

Also, the oxygens surrounding the RE element show an increase in polarizability and covalency up to 30 mol% Na_2O as the AS prove. Since tetrahedrally coordinated oxygens have a higher polarizability than trigonally coordinated oxygens, the increase in polarizability up to 30 mol% is reasonable. The polarizability correlates with the covalency of the metal-oxygen bonds: The more polarizable the oxygens are, the more covalent is the character of the bonds. This is also in accordance with the results obtained by the investigation of the nephelauxetic effect with Nd^{3+}.

Anyway, when all existing Al_2O_3 has been converted to AlO_4 units by Na_2O (in the case of $Al_2O_3 > Na_2O$), the remainder of aluminium, according to Doweidar *et al.* would additionally form AlO_6 in different linkages with the borate units. In the case of all aluminium atoms four-coordinated ($Al_2O_3 < Na_2O$), the addition of further Na_2O only leads to the formation of triclusters containing AlO_4 and BO_4 and hence an increased number of NBOs. As in most of the prepared samples, the molfraction of Al_2O_3 is smaller than the one of Na_2O, the formation of the above mentioned di- and triclusters takes place and hence more NBOs are present. This is also the explanation for the increasing polarizability: The samples 10-75-15, 10-70-20 and 20 – 55 - 25 can all be described by $Al_2O_3 > Na_2O$ and therefore they have quite small AS ratios (about 1.90), which can be explained by the higher symmetry due to the more probable tendency of the formation of AlO_6 units present in different linkages with the borate units. These

results are generally in accordance with the results obtained by the investigation of the nephelauxetic effect: Up to 30 mol% Na_2O the samples also show an increase in covalency.

However, above 30 mol% Al_2O_3 practically all aluminium exists in tetrahedral units and hence no more changes in symmetry take place, as it was proved.

Last but not least, it has to be concluded that, the situation is complex due to the simultaneous use of oxygen for the formation of both AlO_4 in diclusters and triclusters and further, because also a fraction of the BO_4 groups could be included in the triclusters.

The optical basicity shows a continuous increase with increasing Na_2O content. It correlates with the polarizability and the covalency of the oxygens and is a measure for the electron donation ability of the oxygens. As it increases with increasing Na_2O, the electron donation ability also increases. This would also correspond with the observed increase in NBOs.

The densities increase with increasing Na_2O due to the closer packaging of four-coordinated boron units. Nevertheless, they do not show any different behaviour at 30 mol% Na_2O. This leads to the assumption that despite the increase in volume of voids, which is represented by the decrease in packing ratios, the density increases. This can be explained by the sodium moving to interstitials.

Due to the decreasing packing ratio beginning at 15 mol% Al_2O_3 and for higher contents of Al_2O_3, one can assume that the volume of voids in the glasses investigated increases and hence with increasing sodium oxide contents more and more Na^+ change their positions from voids to interstitials. Hence, more voids are built up. With a further increase of the Al_2O_3 content the packing ratio decreases which may be also explained by an increase of the volume of the voids.

The densities show minima at 15 mol% Al_2O_3 for the samples with 20 and 30 mol% Na_2O. This is explained by Doweidar *et al.* with the increase in the fraction $N_3(B)$ with increasing Al_2O_3 concentration. The increase of density above 15 mol% can be related to the formation of triclusters. The maximum in density at about 15 mol% Al_2O_3 and 10 mol% Na_2O can be also related to the formation of triclusters due to the lack of oxygens at low sodium oxide concentrations.

Bibliography

[1] Axinte, E. (2010). Glasses as engineering materials: A review. *Elsevier*, *Materials & Design*, 32, 1721.

[2] Lahoz, F., Pérez-Rodríguez, C., Hernández, S.E. *et al.* (2011). Upconversion mechanisms in rare-earth doped glasses to improve the efficiency of silicon solar cells. *Elsevier, Solar Energy Materials and Solar Cells*, 95, 1671.

[3] Vallet-Regí, M., Victoria Ragel, C., Salinas, A. J. (2003). Glasses with Medical Applications. *European Journal of Inorganic Chemistry,* 129.

[4] Kreidl, N.J.; A dedication to Krogh-Mode: His contribution to the understanding of borate glasses, in Borate Glasses Structure, Properties, Applications, from: Borate glasses, Materials Science Research, 12, Preview, Springer, New York, 1978.

[5] Axinte, E. (2010). Glasses as engineering materials: A review. *Elsevier, Materials & Design*, 32, 1718.

[6] Gatterer, K.; Habilitation treatise: Optical Spectroscopy of Rare-Earth Doped Oxide Glasses, 1, Faculty of Science and Technology, University of Technology, Graz, 1998.

[7] Gaafar, M.S., Abdeen, M. A. M., Marzouk, S. Y. (2010). Structural investigation and simulation of acoustic properties of some tellurite glasses using artificial intelligence technique. *Elsevier, Journal of Alloys and Compounds*, 509, 3566.

[8] García Solé, J., Bausá, L.E., Jaque; D.; An Introduction to the Optical Spectroscopy of Inorganic Solids. 204f., John Wiley & Sons, Ltd, England, 2005.

[9] Gatterer, K., Pucker, G., Fritzer, H.P., Arafa, S. (1994). Hypersensitivity and nephelauxetic effect of Nd(III) in sodium borate glasses. *Journal of Non-Crystalline Solids,*176, 37.Gatterer, K., Pucker, G., Fritzer, H.P. (1996). Structural information in the optical spectra of Eu^{3+} doped glasses from the ternary system Na_2O-B_2O_3-SiO_2. *Physics and Chemistry of Glasses,* 38, 293.

[10] Gatterer, K., Pucker, G., Fritzer, H.P., Arafa, S. (1997). Hypersensitivity of Neodymium Ions in Sodium Borate, Sodium Silicate, and Sodium Borosilicate Glasses. *Second International Conference on Borate Glasses, Crystals and Melts,* 384.

[11] Riedel, E.; Anorganische Chemie. 6, 538ff, de Gruyter, Berlin, New York, 2004.

[12] Gresch, R., Müller-Warmuth, W. (1975). ^{11}B and ^{27}Al NMR Studies of Glasses in the System Na_2O-B_2O_3-Al_2O_3 ("NABAL"). *Journal of Non-Crystalline Solids,* 21.

[13] Doweidar H., Moustafa, Y.M., Abd El-Maksoud, S., Silim, H. (1990). Consideration of the boron oxide anomaly. *Journal of Material Science 25,* 253.

[14] Brill, R.H. (1962). A note on the scientist's definition of glass. *Journal of Glass Studies*, *4,* 129.

[15] Schatt, W.; Einführung in die Werkstoffwissenschaft. 7, 100f., Deutscher Verlag für Grundstoffindustrie GmbH., Leipzig, 1991.

[16] Faupel, F., Frank, W.F.J., Raetzke, K. (2003). Diffusion in Metallic glasses and Supercooled Melts. *Reviews of Modern Physics, 75,* 242f.

[17] Debenedetti, P.G., Stillinger, F.H. (2001). Supercooled liquids and the glass transition. *Nature*, 410, 259.

[18] Vogel, W.; Glaschemie. 3, 1-18, Springer, Berlin, 1992.

[19] Kurkjian, C.R., Prindle, W.R. (1998). Perspectives on the History of Glass. *Journal of American Ceramics Society,* 796f.

[20] Vogel, W.; Glaschemie. 3, 62f., Springer, Berlin, 1992.

[21] Warren, B.E.; (1941). Summary of Work on the Atomic Arrangement in Glasses. *Journal of The American Ceramic Society*, 256.

[22] Gatterer, K.; Habilitation treatise: Optical Spectroscopy of Rare-Earth Doped Oxide Glasses, 5, Faculty of Science and Technology, University of Technology, Graz, 1998.

[23] Zachariasen, W.H. (1932). The Atomic Arrangement in Glass. *Journal of the American Chemical Society,* 3847.

[24] Rao, K.J; Structural Chemistry of Glasses. 1, 23f. Elsevier, Oxford, 2002.

[25] Gatterer, K., Albering, J.; Scriptum: Solid State Spectroscopy, CHE.578, SS.2013

[26] Vogel, W.; Glaschemie. 3,49-55, Springer, Berlin, 1992.

[27] Gatterer, K; Habilitation treatise: Optical Spectroscopy of Rare-Earth Doped Oxide Glasses, 7f., Faculty of Science and Technology, University of Technology, Graz, 1998.

[28] Gatterer, K.; Habilitation treatise: Optical Spectroscopy of Rare-Earth Doped Oxide Glasses, 13, Faculty of Science and Technology, University of Technology, Graz, 1998.

[29] Doweidar, H. (1990). Consideration of the boron oxide anomaly. *Journal of Material Science 25,* 253.

[30] Gatterer, K.; Habilitation treatise: Optical Spectroscopy of Rare-Earth Doped Oxide Glasses, 14f., Faculty of Science and Technology, University of Technology, Graz, 1998.

[31] Kuppinger, C.M., Shelby, J.E. (1985). Viscosity and Thermal Expansion of Mixed-Alkali Sodium- Potassium Borate Glasses. *Journal of the American Ceramic Society*, 68, 463.

[32] Gatterer, K.; Habilitation treatise: Optical Spectroscopy of Rare-Earth Doped Oxide Glasses, 14, Faculty of Science and Technology, University of Technology, Graz, 1998.

[33] Gooding, E.J., Turner, W.E.S. (1934). A study of the series of glasses containing sodium oxide, boric oxide and silica. *Journal of the Society of Glass Technology,* 18, 32.

[34] Biscoe, J., Warren, B.E. (1938). X-ray diffraction study of soda-boric oxide glass. *Journal of the American Ceramic Society,* 21, 2874.

[35] Uhlmann, D.R., Shaw, R.R. (1969). The thermal expansion of alkali borate glasses and the boric oxide anomaly. *Journal of Non-Crystalline Solids,* 1, 347.

[36] R. Gresch, W. Müller-Warmuth (1975). ^{11}B and ^{27}Al NMR Studies of Glasses in the System Na_2O-B_2O_3-Al_2O_3 ("NABAL"). *Journal of Non-Crystalline Solids,* 21, 31ff.

[37] H. Doweidar, Y.M. Moustafa, S. Abd El-Madsoud, H. Silim (2000). Properties of Na_2O-Al_2O_3-B_2O_3 glasses. *Elsevier, Materials Science and Engineering, A301, 207ff.*

[38] J. Zhong, P.J. Bray (1986). *NMR Study of Structure of Sodium Boroaluminate Glass at High Sodium Contents.* Journal of Non-Crystalline Solids 84, 17-25, S. 20.

[39] B.M. Walsh (2005). Judd-Ofelt-Theory: Principles and Practices. *Advances in Spectroscopy for Lasers and Sensing,* 403.

[40] Riedel, E.; Anorganische Chemie. 6, 791, de Gruyter, Berlin, New York, 2004.

[41] Gatterer K.; Habilitation treatise: Optical Spectroscopy of Rare-Earth Doped Oxide Glasses, 30f., Faculty of Science and Technology, University of Technology, Graz, 1998.

[42] Nelson, C., Furukawa, T., White, W.B. (1983). Transition metal ions in glasses: Network modifiers or quasimolecular complexes?. *Materials Research Bulletin, 18,* 959ff.

[43] Neuhold, S.F.; Master's thesis: Mechanism of the "self-reduction" of Eu^{3+} in binary and ternary glasses. 25. Faculty of Science and Technology, University of Technolgy, Graz, 2015.

[44] Atkins P.W.; Physical Chemistry, 5th Edition, 378, Oxford University Press, Oxford, 1983.

[45] Kenyon, A.J. (2002). Recent developments in rare-earth doped materials for optoelectronics. *Progress in Quantum Electronics, 26*, 235

[46] Walsh, B.M. (2005). Judd-Ofelt-Theory: Principles and Practices, *Advances in Spectroscopy for Lasers and Sensing,* 405f.

[47] García Solé, J., Bausá, L.E., Jaque, D.; An Introduction to the Optical Spectroscopy of Inorganic Solids. 200, John Wiley & Sons, Ltd, England, 2005.

[48] Binnemans, K. (2015). Interpretation of europium(III) spectra. *Coordination Chemistry Reviews,* 3.

[49] García Solé, J., Bausá, L.E., Jaque, D.; An Introduction to the Optical Spectroscopy of Inorganic Solids. 203, John Wiley & Sons, Ltd, England, 2005.

[50] J. García Solé, L.E. Bausá, D. Jaque; An Introduction to the Optical Spectroscopy of Inorganic Solids. 200f, John Wiley & Sons, Ltd, England, 2005.

[51] G.H. Dieke, H.M. Crosswhite (1963). The Spectra of the Doubly and Triply Ionized Rare Earths. *Applied Optics, 2/7, 675-686.*

[52] Carnall, W.T., Crosswhite, H., Crosswhite, H.M.; Energy level structure and transition probabilities of the trivalent lanthanides in LaF_3. Appendix IV, 7, Appendix VII, 1, Argonne National Laboratory, Argonne, France, 1977.

[53] Jørgensen, C.K., Judd, B.R. (1964). Hypersensitive pseudoquadrupole transition in lanthanides. *Molecular Physics, 8,* 281.

[54] Gatterer, K.; Habilitation treatise: Optical Spectroscopy of Rare-Earth Doped Oxide Glasses. 28, Faculty of Science and Technology, University of Technology, Graz, 1998.

[55] Reisfeld, R., Zigansky, E., Gaft, M. (2004). Europium probe for estimation of site symmetry in glass films, glasses and crystals. *Molecular Physics, 102,* 1319.

[56] Gatterer, K., Pucker, G., Jantscher, W. *et al.* (1998). Suitability of Nd(III) absorption spectroscopy to probe the structure of glasses from the ternary system $Na_2O-B_2O_3-SiO_2$. *Journal of Non-Crystalline Solids 231,* 192ff.

[57] Pucker, G. *et al.* (1995). Optical investigation of Eu^{3+} in a sodium borosilicate glass: Evidence for two different site distributions. *Physical Review, 53,* 6227.

[58] Jørgensen, C.K. (1962). The Nephelauxetic series. *Progress in Inorganic Chemistry, 4,* 473.

[59] Gatterer, K.; Habilitation treatise: Optical Spectroscopy of Rare-Earth Doped Oxide Glasses. 27f., Faculty of Science and Technology, University of Technology, Graz, 1998.

[60] Gatterer, K., Pucker, G., Fritzer, H.P. (1997). Structural information in the optical spectra of Eu^{3+} doped glasses from the ternary system $Na_2O-B_2O_3-SiO_2$. *Physics and Chemistry of Glasses, 38(6), 293-299.*

[61] Gatterer, K., Pucker, G., Jantscher W. *et al.* (1998). Suitability of Nd(III) absorption spectroscopy to probe the structure of glasses from the ternary system $Na_2O-B_2O_3-SiO_2$. *Journal of Non-Crystalline Solids,* 231, 196.

[62] Gatterer, K., Pucker, G., Jantscher W. *et al.* (1998). Suitability of Nd(III) absorption spectroscopy to probe the structure of glasses from the ternary system $Na_2O-B_2O_3-SiO_2$. *Journal of Non-Crystalline Solids,* 231, 192ff.

[63] Gatterer, K.; Habilitation treatise: Optical Spectroscopy of Rare-Earth Doped Oxide Glasses. 28, Faculty of Science and Technology, University of Technology, Graz, 1998.

[64] Reisfeld, R., Zigansky, E., Gaft, M. (2004). Europium probe for estimation of site symmetry in glass films, glasses and crystals. *Molecular Physics, 102,* 1319.

[65] Gatterer, K., Pucker, G., H.P. Fritzer (1997). Structural information in the optical spectra of Eu^{3+} doped glasses from the ternary system $Na_2O-B_2O_3-SiO_2$. *Physics and Chemistry of Glasses, 38(6), 293-299.*

[66] Binnemans, K. (2015). Interpretation of europium(III) spectra. *Coordination Chemistry Reviews,* 8.

[67] Binnemans, K. (2015). Interpretation of europium(III) spectra. *Coordination Chemistry Reviews,* 20f.

[68] Nazarov, M., Noh, D.Y.; New Generation of Europium and Terbium Activated Phosphors from syntheses to application. 115ff, Pan Stanford Publishing, Singapore, 2012.

[69] Pucker, G., Gatterer, K., Fritzer, H.P. *et al.* (1996). Optical investigation of Eu^{3+} in a sodium borosilicate glass: Evidence for two different site distributions. Physical Review, 53, 6231.

[70] Gatterer, K.; Scriptum: Solid State Spectroscopy, CHE.578, SS.2013.

[71] Gatterer, K. Pcker, G., Jantscher, W. *et al.* (1998). Suitability of Nd(III) absorption spectroscopy to probe the structure of glasses from the ternary system $Na_2O-B_2O_3-SiO_2$. *Journal of Non-Crystalline Solids* 231, 189-199.

[72] Gatterer, K., Pucker, G., Fritzer, H.P., Arafa, S. (1994). Hypersensitivity and nephelauxetic effect of Nd(III) in sodium borate glasses. *Journal of Non-Crystalline Solids 176*, 39.

[73] Gatterer, K.; Habilitation treatise: Optical Spectroscopy of Rare-Earth Doped Oxide Glasses, 26, Faculty of Science and Technology, University of Technology, Graz, 1998.

[74] Hughes, S.W. (2006). Measuring liquid density using Archimedes' principle. *Physics Education*, *41*(5), 446.

[75] LS55 User's Guide. 163ff, Perkin Elmer, Inc., United Kingdom, 2007.

[76] Hofer, J.; Diploma thesis: Fluorescence- and Reflection Spectroscopy of Industrially Relecant Minerals for Automatic Sensor Based Sorting Applications. Institute of Physical and Theoretical Chemistry.

[77] Hardware Guide: High-Performance Lambda Spectrometers, 27ff, Perkin Elmer, Inc., United Kingdom, 2011.

[78] Neuhold, S.F.; Master's thesis: Mechanism of the "self-reduction" of Eu^{3+} in binary and ternary glasses. 49. Faculty of Science and Technology, University of Technolgy, Graz, 2015.

[79] Gatterer, K., Pucker, G., Fritzer, H.P., Arafa, S. (1994). Hypersensitivity and nephelauxetic effect of Nd(III) in sodium borate glasses. *Journal of Non-Crystalline Solids 176*, 39.

[80] Reisfeld, R., Eckstein, Y. (1973). Optical Spectra of Erbium and Thulium in Germanate Glass*. Journal of Non-Crystalline Solids* 12 357-376. S.371]

[81] Duffy, J.A. (1993). A review of optical basicity and its applications to oxidic systems. *Geochimica et Cosmochimica Acta,* 57(16), 3961-3970.

[82] Gatterer, K., Pucker, G., Fitzer, H.P. (1996). Structural information in the optical spectra of Eu^{3+} doped glasses from the ternary system Na_2O-B_2O_3-SiO_2. *Physics and Chemistry of Glasses,* 38, 294.

[83] Gatterer, K., Pucker, G., Jantscher, W., Fritzer, H.P., Arafa, S. (1998). Suitability of Nd(III) absorption spectroscopy to probe the structure of glasses from the ternary system Na_2O-B_2O_3-SiO_2. *Journal of Non-Crystalline Solids,* S. 96,

[84] Nageno, Y., Takebe, H., Morinaga, K. (1993). Correlation between Radiative Transition Probabilites of Nd^{3+} and Composition in Silicate, Borate and Phosphate Glasses. *Journal of the American Ceramic Society.* 76, 3081.

[85] Slater, J.C. (1964). Atomic Radii in Crystals. *The Journal of Chemical Physics*, 41, 10, S.3201.

[86] Atkins, P.W.; Physical Chemistry, 5th Edition, 1006, Oxford University Press, Oxford, 1983.

List of Figures

List of Tables